CHALMERS

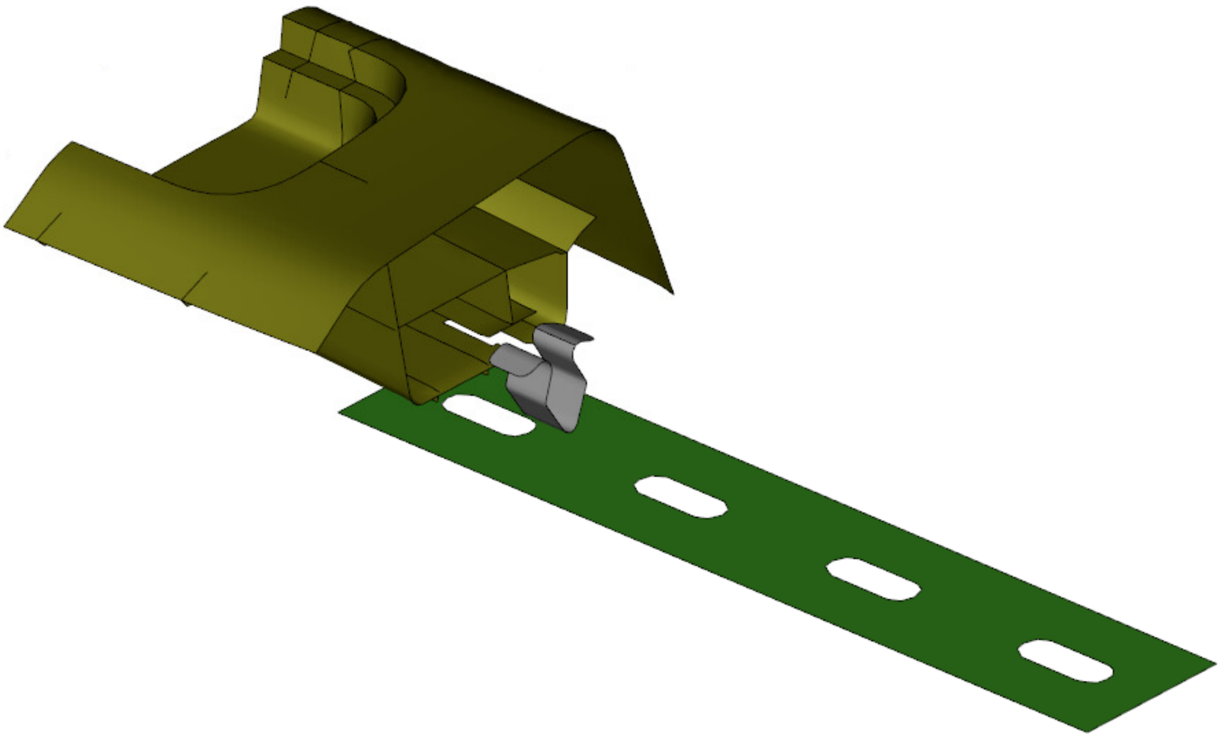

Modelling of the mechanical behaviour of clips for automotive interior panels

Master's thesis in Applied Mechanics

NIKLAS FLÖE

Department of Industrial and Materials Science
CHALMERS UNIVERSITY OF TECHNOLOGY
Göteborg, Sweden 2018

MASTER'S THESIS IN APPLIED MECHANICS

Modelling of the mechanical behaviour of clips for automotive interior panels

NIKLAS FLÖE

Department of Industrial and Materials Science
Division of Material and Computational Mechanics
CHALMERS UNIVERSITY OF TECHNOLOGY

Göteborg, Sweden 2018

Modelling of the mechanical behaviour of clips for automotive interior panels
NIKLAS FLÖE

Master's thesis 2018
Department of Industrial and Materials Science
Division of Material and Computational Mechanics
Chalmers University of Technology
SE-412 96 Göteborg
Sweden
Telephone: +46 (0)31-772 1000

Cover:
The cover figure show the FE-model that was used to evaluate the force contribution from the clip for assembly and disassembly of the front sill moulding.

Chalmers Reproservice
Göteborg, Sweden 2018

Modelling of the mechanical behaviour of clips for automotive interior panels
Master's thesis in Applied Mechanics
NIKLAS FLÖE
Department of Industrial and Materials Science
Division of Material and Computational Mechanics
Chalmers University of Technology

Abstract

In the automotive industry many different types of clips are used to attach components. Clips enable an easy assembly of components and gives a clean finish since they provide attachments invisible to the customer. The design of the clips affect how attached components move relatively as they are exposed to external loads, for example when the temperature in the vehicle rises. The design also determine the amount of manual force that is required for assembly and disassembly of attached components and therefore affects the ergonomic aspects of these processes. The purpose of this work is to study the mechanical behaviour of a metal clip used to attach interior plastic panels at Volvo Car Corporation (Volvo Cars). This type of clip is widely used to attach different interior panels including the front sill moulding to the car body. The clip together with the front sill moulding is numerically studied by use of the finite element method (FEM).

A method to numerically predict the behaviour of the clip in terms of sliding capability and stiffness is developed. The results show that when the clip slides there are two sliding-phases with different force levels. First there is sliding between clip and panel and then sliding between clip and bracket. The effects of various friction coefficients between parts are studied and a combination of friction coefficients that correlate well to measured sliding capability is presented. The behaviour in terms of torsional stiffness in the clip joint was discovered to be non-linear for rotations around all axes. Furthermore a parameter study on torsional stiffness is carried out to establish the influence of various parameters.

Also a method to numerically evaluate the force required for assembly of the front sill moulding is developed. The method includes geometries and boundary conditions based on previously performed mechanical testing where a part of the front sill moulding together with one clip were included. Results show that the force contribution from the clip during assembly have two peak values, the first one due to sticking friction and the second one due to compression of the clip waist. The effects of varying hole sizes are evaluated and the results correlate well to previously performed physical tests. A parameter study is carried out on varied friction coefficients and velocity of assembly. The results show that when using the friction coefficients found from correlation of sliding capability, the assembly force is best captured as compared to physical tests. Furthermore, the effect on assembly force when including the complete front sill moulding and three clips was numerically investigated. For the first clip connection the behaviour during assembly is similar to the behaviour when only including a part of the panel. This result indicate that a simplified method is sufficient in order to numerically capture the contribution to assembly force from the clip.

Numerical evaluation of force required for disassembly was proven difficult without modelling residual stresses and hardening due to manufacturing of the clip. Using elastoplastic material data for the clip the disassembly force is underestimated and when using linear elastic steel the disassembly force is overestimated.

Keywords: Finite element method, vehicles, clips, interior panels, lateral stiffness, torsional stiffness, sliding capability, assembly force, disassembly force

Preface

This master thesis is the final part of my Master's degree in Applied Mechanics at Chalmers University of Technology. The project work was carried out at the department of CAE Closure, Interior and Exterior at Volvo Car Corporation in Torslanda. My supervisors at Volvo Cars have been MSc. Kaveh Behbahani and MSc. Marcus Hammar. My examiner at Chalmers University of Technology was Dr. Mats Ander.

Acknowledgements

I would like to express my sincerest gratitude to my supervisors Kaveh Behbahani and Marcus Hammar for guiding me in the right direction and for answering all my questions throughout this project. Also I would like to thank my examiner Mats Ander for providing valuable input at our weekly Skype meetings. I would also like to thank Louise Wetterberg, Sara Helmrot, Camilla Schaurig, Rasmus Behrens and Magnus Bergman for sharing their knowledge and test data related to the assembly process of interior panels.

I would also like to express gratitude to Joakim Asklund at Simulia for providing support related to simulations in Abaqus. Lastly, I would like to thank everyone at the department of CAE Closure, Interior & Exterior for a warm welcome to the office.

Nomenclature

$\boldsymbol{\sigma}$	Second order stress tensor	$[MPa]$
$\boldsymbol{\sigma}_{dev}$	Second order deviatoric stress tensor	$[MPa]$
$\boldsymbol{f}_{ext}$	External force vector	$[N]$
$\boldsymbol{f}_{int}$	Internal force vector	$[N]$
$\boldsymbol{g}$	Residual force vector	$[N]$
$\boldsymbol{I}$	Second order identity tensor	$[-]$
$\boldsymbol{K}_T$	Tangent stiffness matrix	$[MPa]$
$\boldsymbol{M}$	Lumped mass matrix	$[kg]$
$\boldsymbol{u}$	Displacement	$[mm]$
$\ddot{\boldsymbol{u}}$	Acceleration	$[\frac{mm}{s^2}]$
$\delta\boldsymbol{u}$	Incremental displacement vector	$[mm]$
Δt	Increment time	$[s]$
$\dot{\boldsymbol{u}}$	Velocity	$[\frac{mm}{s}]$
ϵ	Strain	$[-]$
ϵ_{pen}	Penalty stiffness factor	$[-]$
μ	Friction coefficient	$[-]$
Π_{pen}	Contribution to energy due to contact penalty	$[kg\frac{mm^2}{s^2}]$
σ_0	Yield limit	$[MPa]$
$\sigma_{e,vM}$	Effective Mises stress	$[MPa]$
τ_{max}	Maximum allowed shear stress for sticking between two surfaces	$[MPa]$
θ	Rotational angle	$[rad]$
$c[u]$	Gap between interacting surfaces	$[mm]$
E	Youngs modulus	$[MPa]$
F_a	Applied force	$[N]$
G	Shear modulus	$[GPa]$
k	Iteration number	$[-]$
k_θ	Torsional stiffness	$[\frac{Nmm}{rad}]$
k_y	Lateral stiffness	$[\frac{N}{mm}]$
L_g	Clip gap length	$[mm]$
L_w	Clip waist length	$[mm]$
L_{avg}	Average torque arm length	$[mm]$
M_a	Applied torque	$[Nmm]$
P	Contact pressure	$[MPa]$
q_x, q_y, q_z	Rotational degrees of freedom	$[-]$
u_x, u_y, u_z	Translational degrees of freedom	$[-]$
i	Increment number	$[-]$

Contents

1 Introduction

This study deals with a finite element analysis (FE-analysis) of the behaviour of a metal clip widely used in vehicles at Volvo Cars. In this chapter the background, purpose, methodology and limitations of the project is explained.

1.1 Background

In the automotive industry many different types of clips are used to attach different components. Clips could either be integrated in the structure of the component or be separate items. The purpose of using clips for these applications is that they enable an efficient assembly in the factory and, in contrast to using bolts, clips enables a clean finish to components since they are invisible to the customer. A common application for clips is to attach interior panels to each other as well as to the car body. In this project a metal clip which is, among other applications, used to attach a type of panel called the front sill moulding to the car body is studied. This panel is located in the lower front of the vehicle and highlighted in Figure 1.1 and contains three clip connections. Furthermore, there are three guiding pins for which the purpose is to align the front sill moulding in the correct position during assembly.

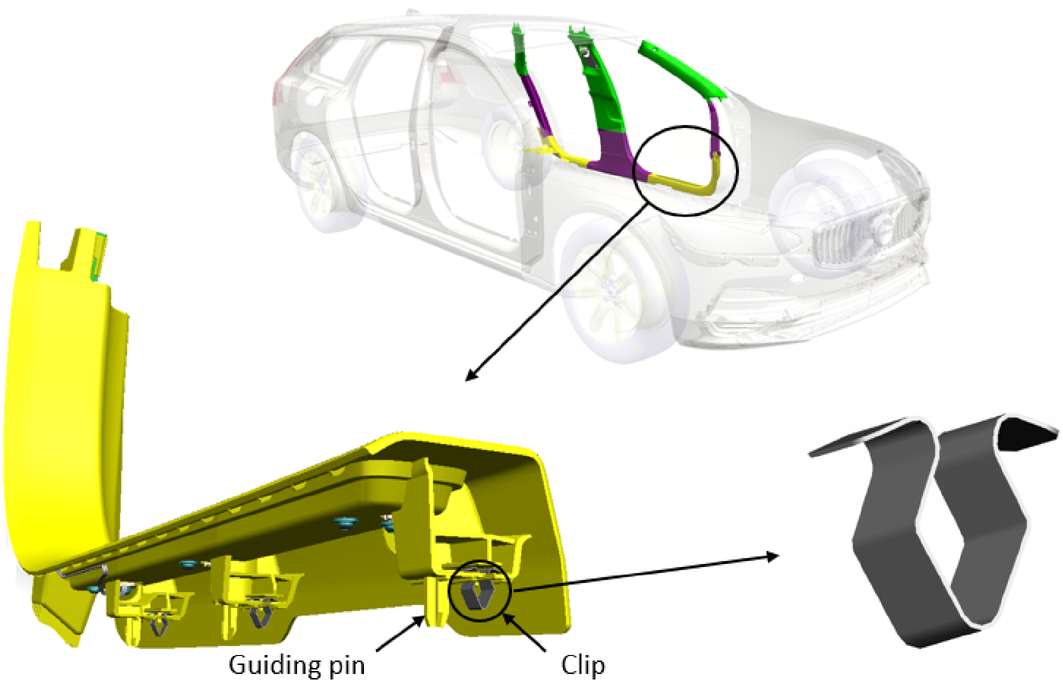

Figure 1.1: *Interior panels connected to the car body by use of clips. The front sill moulding with the studied clip. Note the guiding pin located beside the clip.*

The front sill moulding is attached to three metal brackets which are spot-welded onto the car body. In each of these brackets there is an oval hole for the clip and a hole for the guiding pin, see Figure 1.2a. The purpose of the design of this type of clip is to enable an easy assembly of parts but to still maintain a high force required for disassembly so that the parts connected by this type of clips stay in place. The difference in force for assembly and disassembly is obtained by the different angles on the lower and upper part of the clip. These angles together with geometries of the CAD-model of the clip can be seen in Figure 1.2b.

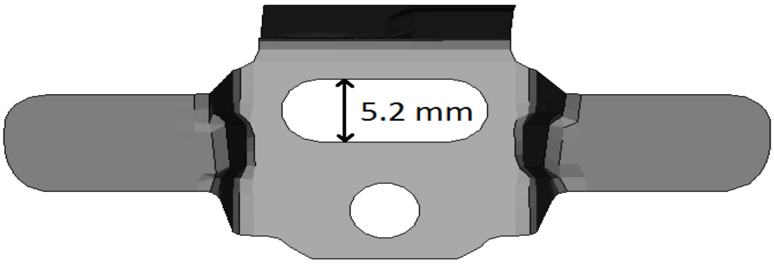

(a) *The bracket that the front sill moulding is mounted onto. The nominal width of the hole where the clip goes in to is marked.*

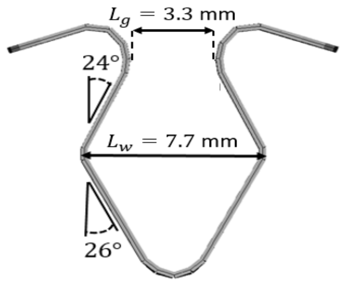

(b) *Relevant geometries of the clip.*

Figure 1.2: *Geometries of the bracket and the clip.*

In addition to the effects on assembly and disassembly force the design of the clip also affects how attached components move relative to each other as they are exposed to external loads. When a car is parked in the sun on a warm day, temperature inside the vehicle rises which causes plastic components such as interior panels to expand which induce sliding and rotation relative to the brackets.

At Volvo Cars there is an interest in being able to predict the behaviour of such clips, before physical parts are available, by using FEM. Understanding of the physical nature of such components bring clarity to how parts connected by clips move relative to each other. It also brings clarity to whether the assembly process is ergonomically satisfying for the assembler and also makes it possible to identify parameters that may cause ergonomic issues.

1.2 Purpose

This master thesis has two main purposes. The first one is to develop a method to numerically predict the mechanical properties of the clip including lateral stiffness, sliding capability and torsional stiffnesses by development of a detailed finite element model (FE-model). The second purpose is to develop a method to numerically predict the force contribution by the clip during assembly and disassembly of the front sill moulding.

1.3 Method

The mechanical properties of the clip are evaluated by carrying out a progressive finite element analysis (FE-analysis). For this purpose a detailed FE-model is developed and an accurate representation of the clip is found by evaluation of lateral stiffness and correlation to previously performed physical testing [1]. The results are then used as input for evaluation of sliding capability. The FE-model is calibrated so that the sliding capability correlate well to previously performed physical tests and the results are used as input for evaluation of torsional stiffness.

The force contribution by the clip during assembly and disassembly is evaluated by development of a FE-model based on geometries used during previously performed mechanical testing at Volvo Cars. This FE-model is used to evaluate the assembly force for varying hole sizes and calibrated to correlate well to measurement data [10]. The force required for disassembly is then evaluated by using the assembled state as initial state and correlated to data provided by the supplier of the clip [4].

During this project Abaqus/Standard [8] and Abaqus/Explicit [7] have been used for finite element calculations, Ansa [2] has been used for pre-processing and Meta [3] together with Matlab [12] have been used for post-processing of results.

1.4 Limitations

The assembly of complete panels onto the car body is a complex process. The manual force that is required for assembly is affected by many different factors, e.g. rubber sealing between parts and peeling of plastic material of the guiding pins. The focus of this master thesis was to evaluate the mechanical behaviour of clips in particular, thus none of the above described phenomena have been modelled or analyzed.

To validate the simulation models, data from mechanical tests performed at Volvo Cars have been used and these data are limited and of varying accuracy. Even though data may be insufficient for complete validation of simulation models, the master thesis work was limited to use by the existing data only.

Residual stresses and hardening of material from manufacturing of parts are not accounted for in this project. However, such phenomena are discussed as possible error sources.

Simulations are only carried out with material data for room temperature.

Due to confidentiality of data, including reports, in Volvo Cars, material grade will not be presented by detail in this report. The same limitation is valid for correlation of achieved results related to assembly and disassembly force against Volvo Cars internal as well as external suppliers physical tests.

1.5 Ethical aspects

During this project simulations of the assembly process of interior panels are carried out. The results provided in this thesis may be used in further work related to improving the ergonomic aspects of this process which can be seen as a positive ethical aspect. However, the people working with this process on a daily basis should be included in a possible change in work procedure.

2 Theoretical framework

In this chapter the theory that is used throughout the report is described. This chapter serves as a reference for the reader when explaining the methodology as well as the behaviour observed from the results. The coordinate system that is used to describe directions can be seen in Figure 2.1. Translational and rotational degrees of freedom (DOF) are referred to as u_x, u_y, u_z and q_x, q_y, q_z respectively.

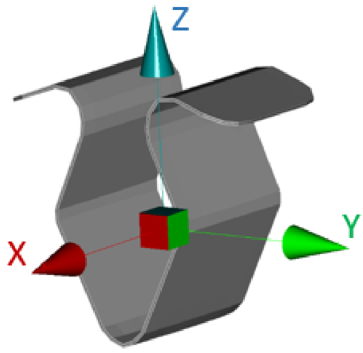

Figure 2.1: *The coordinate system that is used to describe directions.*

2.1 Contact enforcement methods

In Abaqus numerous different contact enforcement methods are available. The ones that have been used during this project are described below.

2.1.1 Linear penalty method

The linear penalty method consists of adding a contribution to the energy if the gap, c[u], between two interacting surfaces is below zero, i.e. in contact. The contribution to the energy is given by [17]:

$$\Pi_{pen} = \epsilon_{pen}[c(u)]^2 \tag{2.1}$$

where ϵ_{pen} is the penalty parameter which can be seen as the stiffness of a spring that is added between the interacting surfaces. The relationship between contact pressure and overclosure is linear when using the linear penalty method, which results in a constant penalty parameter, as explained in chapter 38.1.2 in [5]. This contact enforcement method is efficient in terms of computational time since no expansion of the stiffness matrix is required, instead stiffness is added to already existing components.

2.1.2 Nonlinear penalty method

The nonlinear penalty method uses the same theory as the linear penalty method, however the relationship between the pressure and overclosure is nonlinear. Using this method Abaqus will choose an initial penalty stiffness factor which, in opposite to the linear penalty method, increases linearly as surfaces interact as explained in chapter 38.2.3 in [5].

2.2 Coupling constraints

Two types of coupling constraints have been used when applying boundary conditions during modelling in Abaqus, kinematic and distributing coupling. The definition of a kinematic coupling is that a set of nodes is coupled to the rigid body motion of a reference node. A distributing coupling is coupled to the rigid body motion of a reference node as well, however in an average sense as discussed in chapter 35.3.2 in [5].

2.3 Constitutive modelling

When defining the properties of a material one has to define a constitutive model, i.e. a relationship between stress, σ, and strain, ϵ. The constitutive models that have been used in this project are isotropic linear elasticity and isotropic elastoplasticity.

The relationship between stress and strain for an isotropic linear elastic material is governed by Hooke's generalized law and dependent on the Young's modulus, E, and Poisson's ratio, ν. The strains when no temperature variation is present are given by Equation 2.2 [15]:

$$\begin{bmatrix} \varepsilon_{11} \\ \varepsilon_{22} \\ \varepsilon_{33} \\ \gamma_{12} \\ \gamma_{13} \\ \gamma_{23} \end{bmatrix} = \begin{bmatrix} 1/E & -\nu/E & -\nu/E & 0 & 0 & 0 \\ -\nu/E & 1/E & -\nu/E & 0 & 0 & 0 \\ -\nu/E & -\nu/E & 1/E & 0 & 0 & 0 \\ 0 & 0 & 0 & 1/G & 0 & 0 \\ 0 & 0 & 0 & 0 & 1/G & 0 \\ 0 & 0 & 0 & 0 & 0 & 1/G \end{bmatrix} \begin{bmatrix} \sigma_{11} \\ \sigma_{22} \\ \sigma_{33} \\ \sigma_{12} \\ \sigma_{13} \\ \sigma_{23} \end{bmatrix} \tag{2.2}$$

where $G = E/2(1+\nu)$ is the shear modulus. Isotropic elastoplasticity means that a material is isotropic linear elastic up to a certain amount of stress, σ_0, where plasticity occur. In Abaqus this limit is for the multiaxial case, for a rate independent material, defined by the effective von Mises stress, $\sigma_{e,vM}$, and given by:

$$\sigma_0 = \sigma_{e,vM} = \sqrt{\frac{2}{3}\boldsymbol{\sigma}_{dev} : \boldsymbol{\sigma}_{dev}} \tag{2.3}$$

where $\boldsymbol{\sigma}_{dev}$ is the deviatoric stress tensor given by:

$$\boldsymbol{\sigma}_{dev} = \boldsymbol{\sigma} - \frac{1}{3} trace(\boldsymbol{\sigma})\boldsymbol{I} \tag{2.4}$$

where $\boldsymbol{\sigma}$ is the stress tensor and $\boldsymbol{I}$ is the second order identity tensor. When using an isotropic hardening model σ_0 increases uniformly in all stress directions as plasticity occur, as discussed in Chapter 23.2.1 in [5].

2.4 Friction

The force required for sliding of the panel relative to the bracket as well as the assembly and disassembly process is highly dependent on frictional forces between parts. The frictional force that acts on a part is dependent on the normal force and the friction coefficient between the two interacting parts.

In Abaqus Coulomb friction is used to define when two interacting surfaces are sticking or sliding. By use of this theory the transition point between sticking and sliding is defined by a maximum shear stress, τ_{max} between the surfaces. This shear stress is defined as a fraction of the contact pressure:

$$\tau_{max} = \mu P_{cont} \tag{2.5}$$

where μ is the friction coefficient and P_{cont} is the contact pressure. The contact pressure is a function of the normal force, F_N, between the interacting surfaces and the area of contact. For more information about the friction model the reader is referenced to chapter 5.2.3 in [6].

2.5 Mechanical properties of the clip

In this project the lateral stiffness, k_y, and the torsional stiffness, k_θ, of the clip are evaluated. The lateral stiffness is defined as the slope between force required to compress the clip in Y-direction, F_y, versus the compression distance, u_y. It is calculated in the same way as the stiffness of a linear elastic spring:

$$\Delta F_y = k_y \Delta u_y \rightarrow k_y = \frac{\Delta F_y}{\Delta u_y} \tag{2.6}$$

The variables used to calculate lateral stiffness can be seen in Figure 2.2.

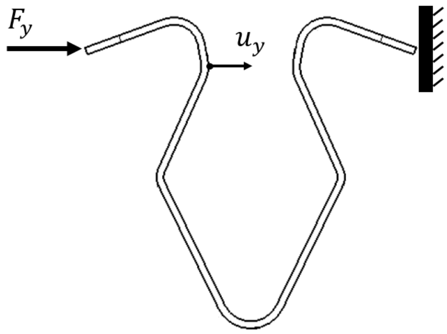

Figure 2.2: *Visualization of the variables used to calculate lateral stiffness.*

The torsional stiffness is defined as the slope between applied torque, M_a, and rotational angle, θ. It is calculated in the same way as the stiffness of a torsional spring:

$$\Delta M_a = k_\theta \Delta\theta \rightarrow k_\theta = \frac{\Delta M_a}{\Delta\theta} \tag{2.7}$$

The torque is calculated by using the average torque arm length, L_{avg}=$(L_1 + L_2)/2$, and the applied Force, F_a:

$$M_a = F_a L_{avg} \tag{2.8}$$

As an example the variables used to calculate torsional stiffness for rotation around Z is shown in Figure 2.3.

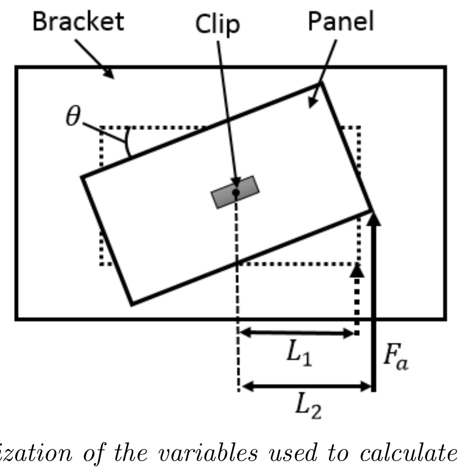

Figure 2.3: *Visualization of the variables used to calculate torsional stiffness.*

2.6 Assembly and disassembly force

During assembly and disassembly of the front sill moulding the clip is subjected to forces arising as contact between the interacting parts occur. Load is applied to the panel and as a consequence the clip is subjected to a force acting in the loading direction. When the clip is in contact with the bracket it is subjected to a force with normal direction to the contact area and consequently also frictional forces. The first step during both assembly and disassembly is that the gap at the upper part of the clip is closed. At this stage, the angle between clip and bracket have been reduced from 26° to 15° during assembly and increased from 24° to 34° during disassembly, see Figures 2.4a and 2.4b respectively. At this point the clip waist, L_w, is 6.0 mm thus a further compression of 0.8 mm is required for successful assembly or disassembly through the bracket hole. Since the angle between clip and bracket is smaller during assembly the clip is subjected to less resistance as compared to disassembly and consequently less force is required.

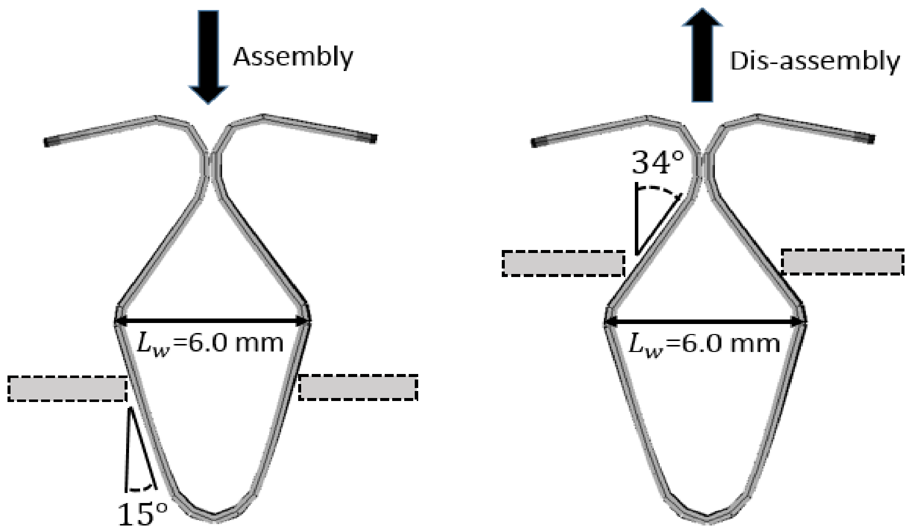

(a) *Clip in contact with the bracket during assembly.* (b) *Clip in contact with the bracket during disassembly.*

Figure 2.4: *Angles between clip and bracket at the stage where the clip gap have been closed during assembly and disassembly.*

2.7 Material data

The material that is used for the clip is a spring steel, the front sill moulding is manufactured with ABS-plastic and the material used for the brackets is steel. A summary of the Young's modulus, E, yield limit, σ_y, and ultimate tensile strength, σ_u, at room temperature for each material can be seen in Table 2.1. For all materials isotropic linear elasticity with isotropic hardening plasticity is implemented.

Table 2.1: Yield limit and ultimate tensile strength for materials used for the different parts.

Component:	Material:	E [GPa]:	σ_y [MPa]:	σ_u [MPa]:
Clip	Spring steel	201	385	703
Bracket	Steel	210	358.5	779.7
Panel	ABS-plastic	2.2	32.02	96.07

3 Evaluation of mechanical properties of the clip

In this chapter the development of a method to predict mechanical properties of the clip including lateral stiffness, sliding capability and torsional stiffness is explained. Furthermore numerical results from a progressive FE-analysis and correlation to mechanical tests previously performed at Volvo Cars are presented.

3.1 Previous work

The mechanical properties of the omega clip have previously been measured in simple physical testing at Volvo Cars [1]. During these tests the lateral stiffness, sliding capability and torsional stiffness were evaluated. The tests where performed on a part of an interior panel called the upper B-pillar which has some geometrical differences as compared to the front sill moulding that is modelled in this thesis work. The results acquired from these measurements are used for correlation and validation of the simulation model. However, geometrical differences for the two interior panels can be considered as a potential error source in the correlation study. For example, when evaluating torsional stiffness of the clip the panel is rotated relative to the car body which would give a point of rotation which is highly dependent on the geometry of the panel. Furthermore the test data that are used for correlation are an average of multiple measurements with a wide spread between tests in some cases, thus caution has to be taken when deeming the test results accurateness.

Since the goal was to develop a method to predict the mechanical properties of the clip and to validate simulation results by use of the measured data the simulation setup was based on the conditions during tests.

3.2 Methodology

The mechanical properties of the clip were evaluated by performing a progressive FE-analysis. This means that results acquired from one step in the analysis are used in the next step.

First a detailed FE-model was developed to be used for evaluation of the mechanical properties. The next step was to get an accurate representation of the clip by correlating lateral stiffness to measured data. The representation of the clip was then implemented in the FE-model and the sliding capability were evaluated and calibrated to correlate well to physical measurement. Lastly the torsional stiffnesses of the clip were evaluated and compared to measured data and a parameter study was performed. An overview of the methodology can be seen in Figure 3.1.

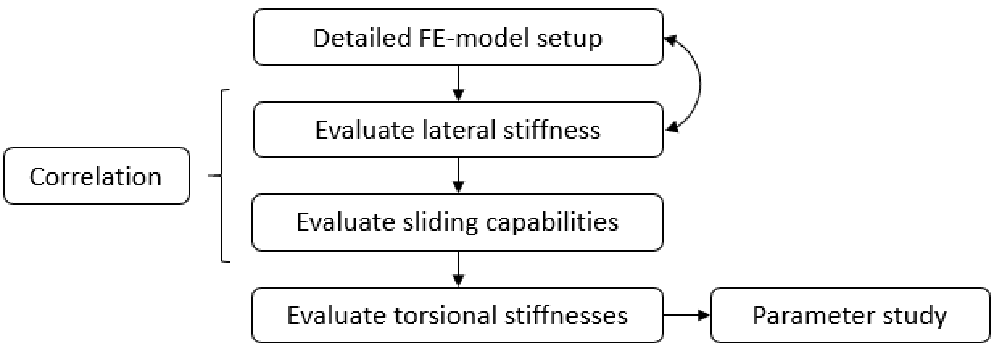

Figure 3.1: *The methodology used to evaluate the mechanical properties of the clip.*

3.3 FE-model setup

To fully capture the behaviour of the omega clip in terms of sliding capability and stiffness properties a detailed FE-model was developed to be used in a static analysis with implicit time integration. The procedure for this analysis type is described in Appendix A. The guiding pin which in reality is located beside the clip has been excluded to fully allow sliding and rotation for the front sill moulding relative to the bracket. For meshing of the front sill moulding, 10-node quadratic tetrahedral solid elements denoted C3D10H in Abaqus, were used. For the clip general purpose shell elements, denoted S4 and S3R in Abaqus, were used. The element types used for the bracket are the same as for the clip, however the area closest to the clip was meshed with 8-node hexahedral continuum shell elements, denoted SC8R in Abaqus [5]. The mesh with corresponding element types that have been used for each part can be seen in Figure 3.2. The target element sizes were 2 mm for the front sill moulding and bracket and 1 mm for the clip. The bracket is in reality connected to the car body by spot welds. In the FE-model the constraint for the bracket has been modelled with a fully constrained kinematic coupling. There is also a kinematic coupling located on the front sill moulding for which the purpose is to add constraints specific to each load case. In addition to this the front sill moulding is constrained in DOF u_z by use of a gravity load.

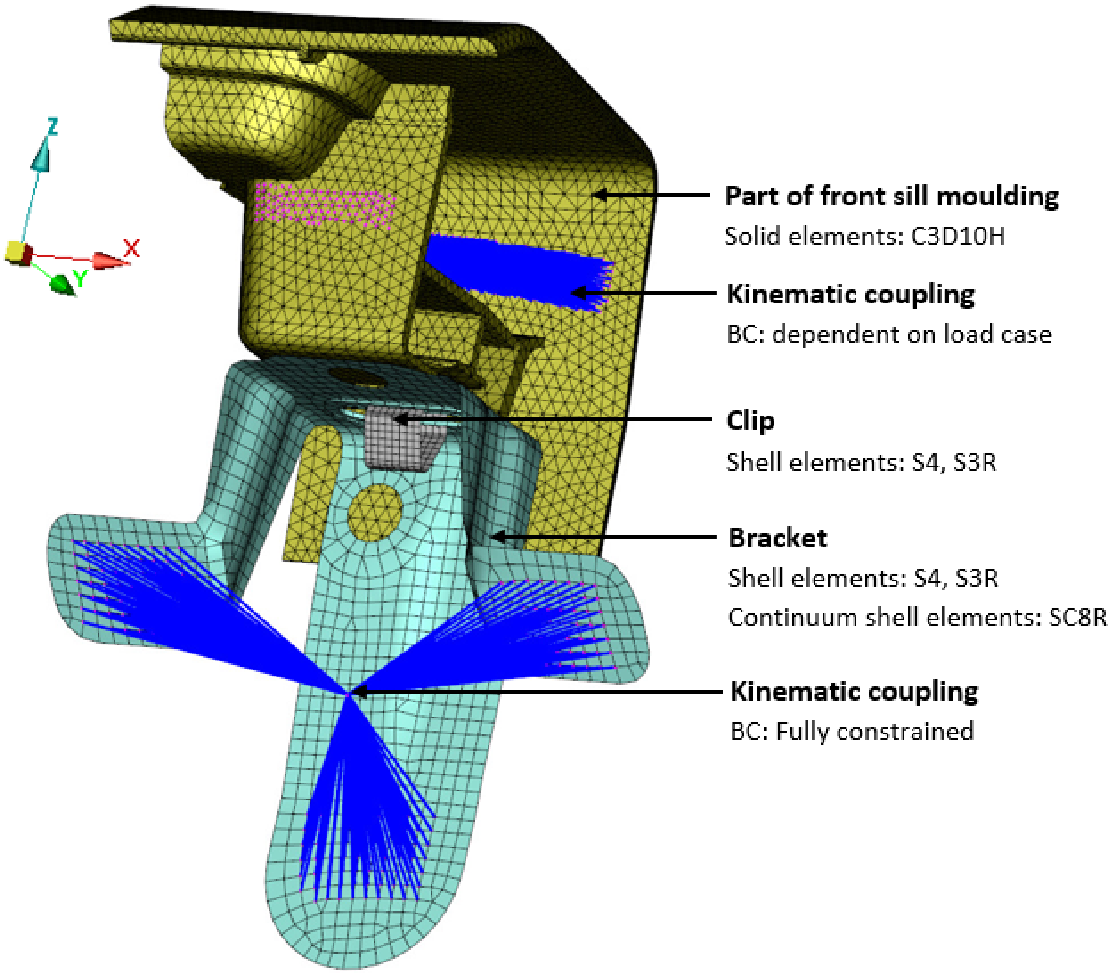

Figure 3.2: *The mesh of the detailed FE-model with the different parts as well as element types. The kinematic couplings that have been used for constraints of the panel and the bracket are also visible.*

For all contact pairs a linear penalty method was used to enforce contact. The initially chosen friction coefficients between the different interacting surfaces were chosen based on values used in previous work [14]. They can be seen in Table 3.1.

Table 3.1: The initially chosen friction coefficients between the interacting parts of the detailed FE-model. Values are based on previous work about metal clips [14].

Interaction:	Materials:	Friction coefficient:
Clip-Panel	Spring steel-ABS	0.30
Bracket-Panel	Steel-ABS	0.30
Clip-Bracket	Spring steel-Steel	0.31

When the clip is in position between the bracket and panel it has some strain due to the fact that the function of the clip is to keep the two parts together. When setting up the FE-model this means that there is penetration present between the clip and the two surrounding parts, see Figure 3.3a. This penetration was numerically solved by using interference fit in Abaqus as an initial simulation step. By using this approach Abaqus gradually resolves the overlap during the first step of a simulation by adding strain and corresponding stress to the desired part, in this case the clip, as described in chapter 36.2.4 in [5]. At this step some convergence difficulties occurred, and to solve this the penalty stiffness factor had to be scaled by a factor of 0.1. This would mean that a "softer" contact condition is used and small penetration between parts is expected. The clip after that the initial penetration was resolved can be seen in Figure 3.3b.

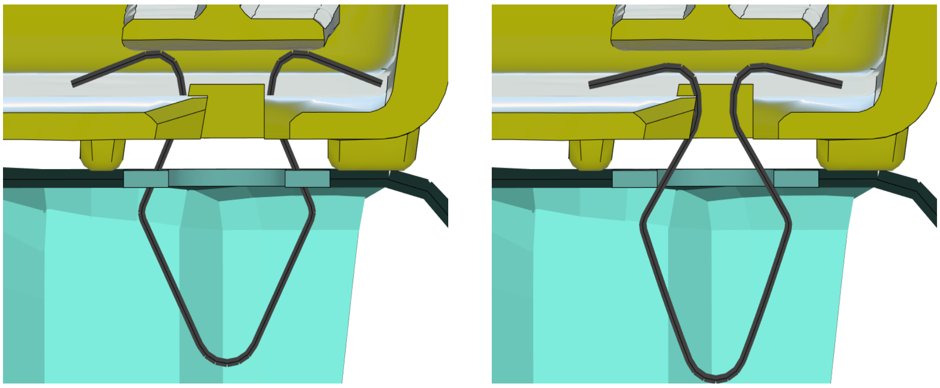

(a) *The clip before the initial penetration was resolved.*

(b) *The clip after the initial penetration was resolved.*

Figure 3.3: *The clip before and after initial penetration was resolved.*

3.4 Lateral stiffness

Before implementing load cases for evaluating sliding capability and torsional stiffnesses the lateral stiffness of the clip was evaluated for which the purpose was to find an accurate representation of the clip and to evaluate the validity of available material data.

Previous testing performed at Volvo Cars suggest an average lateral stiffness of 2.66 N/mm for the tested clip specimens and that the relationship between force and gap-change is linear. In order to test the FE-model in regard of this property a simulation was set up including only the clip. The boundary conditions for this simulation were based on the setup during physical testing, i.e., by constraining the nodes of one end of the clip from movement and then prescribing a displacement to the clip at the other end so that self-contact is reached, as visualized in Figure 3.4.

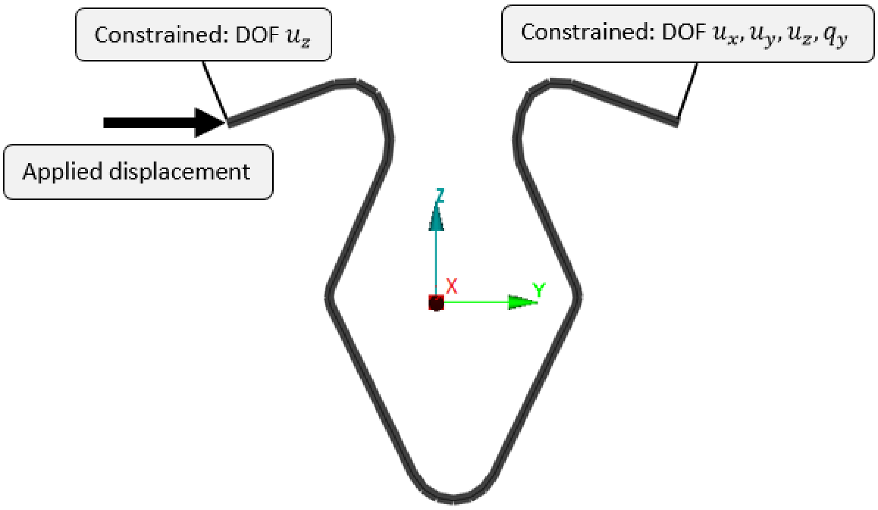

Figure 3.4: *The boundary conditions used for evaluating lateral stiffness of the clip.*

Results from this simulation show that the force versus gap-change is non linear. This is due to plasticity that occur in the material and as a result the gap size is changed from 3.3 mm to 2.6 mm after unloading. However results from physical tests suggest a constant lateral stiffness [1]. The resulting force versus gap-change curve from the simulation as well as the von Mises stresses at maximum displacement can be seen in Figures 3.5a and 3.5b respectively.

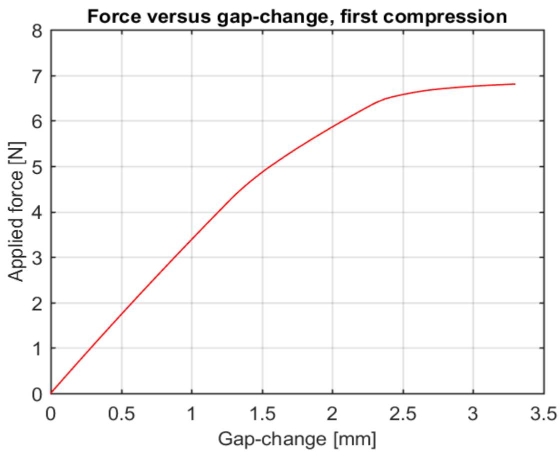

(a) *The resulting force versus gap-change curve when initially compressing the clip.*

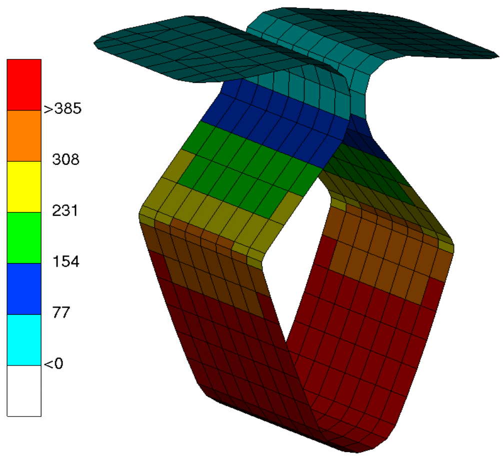

(b) *The von Mises stresses in the clip at maximum compression [MPa]. Note the area with stresses above the yield limit.*

Figure 3.5: *Applied force during first compression and von Mises stresses in the clip at maximum compression.*

In order to achieve a constant lateral stiffness of the clip a simulation step was added where the clip was compressed one additional time after the first compression. The resulting force versus gap-change for the second compression compared to the average value from physical measurements can be seen in Figure 3.6. Due to the isotropic hardening that occur in the first compression the force versus gap-change is now linear.

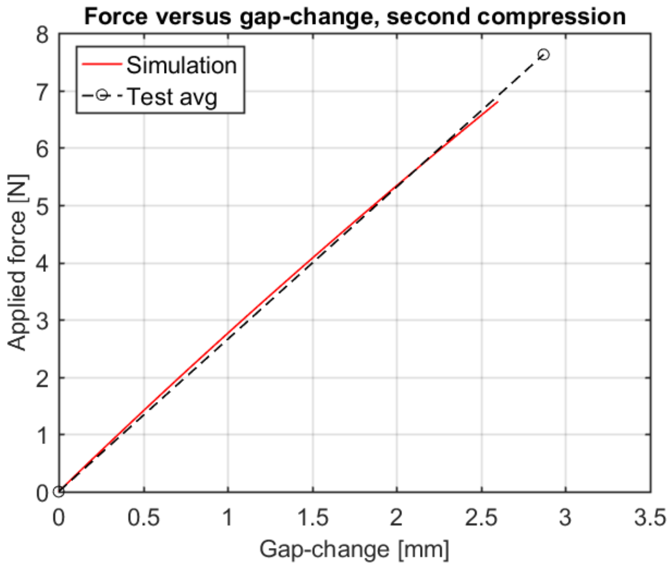

Figure 3.6: *The resulting force versus gap-change during the second compression of the clip compared to suggested constant lateral stiffness from physical measurements [1].*

The lateral stiffness during the second compression is 2.62 N/mm which is close to the value of this property suggested from physical tests. With this result in regard two simulation steps were added after the interference fit where the clip was compressed until self contact was reached and then released in order to achieve a lateral stiffness that correlate well to that found in physical measurements.

As previously discussed the gap size after the first compression is changed from 3.3 to 2.6 mm due to plastic deformations. The clip specimens used during testing had an average gap size of 2.87 mm and a spread between 2.5 and 3.1 mm. The gap size of the implemented representation of the clip deviates from the average test value, however it lies within the range of spread of clip specimens.

3.5 Sliding capability

The sliding capability is defined as how much force that is required for the front sill moulding to slide in local X direction relative to the bracket.

The sliding behaviour of the FE-model was evaluated by prescribing a displacement in local X direction to the panel. The area of the panel where the displacement is applied can be seen in Figure 3.7. In addition to this the kinematic coupling node located at the upper part of the panel, see Figure 3.2 in Chapter 3.3, was constrained from movement in DOF u_y and q_z.

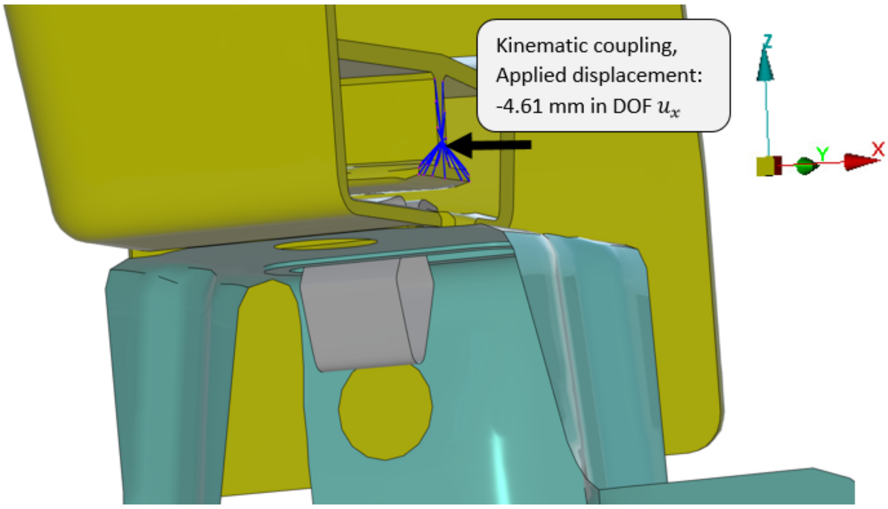

Figure 3.7: *The nodes where the displacement of the panel was applied.*

In tests previously performed at Volvo Cars it was noticed that the sliding behaviour has two phases; one where the clip slides relative to the panel and one where the clip slides relative to the bracket [1]. These two sliding-phases were captured during simulations and can be seen in Figures 3.8a, 3.8b and 3.8c.

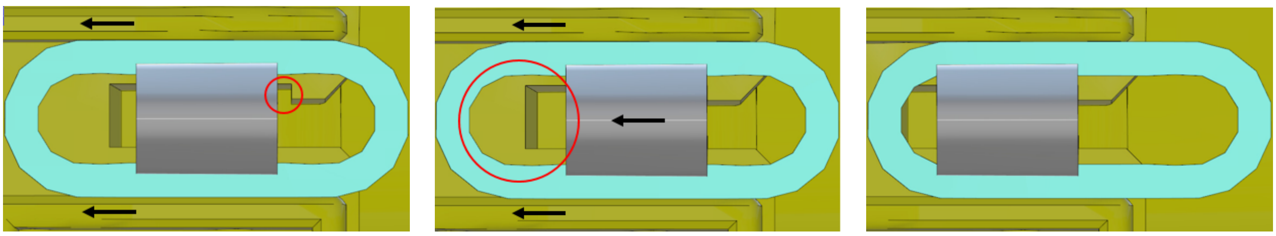

(a) *Start of sliding between clip and panel.* (b) *Start of sliding between clip and bracket.* (c) *End of sliding.*

Figure 3.8: *Sliding along local X visualized. The turquoise colored part represent the elements of the bracket closest to the hole. The yellow part represents the panel and the grey part is the clip. The gap shown in (a) is closed after sliding between clip and panel and the gap shown in (b) is closed after sliding between clip and bracket.*

The purpose of this analysis was to evaluate the force required for sliding along local X and to find suitable friction coefficients between parts so that the behaviour observed during tests is captured. The force required for sliding was evaluated by extracting the reaction force at the coupling node where displacement was applied. A first simulation was run where the initially chosen friction coefficients, see Table 3.1 in Chapter 3.3, were used. In order to capture the sensitivity of the different friction coefficients three additional simulations were carried out where one of the friction coefficients was altered in each simulation. The goal was to find a suitable set of friction coefficients based on the results from this sensitivity analysis by correlation to physical test results.

3.5.1 Numerical results

The resulting force that is required for sliding along local X for initial parameters as well as for decreased friction coefficients between parts can be seen in Figure 3.9. When reducing the friction coefficient between clip and panel the two sliding phases were not captured, and thus is not included in Figure 3.9.

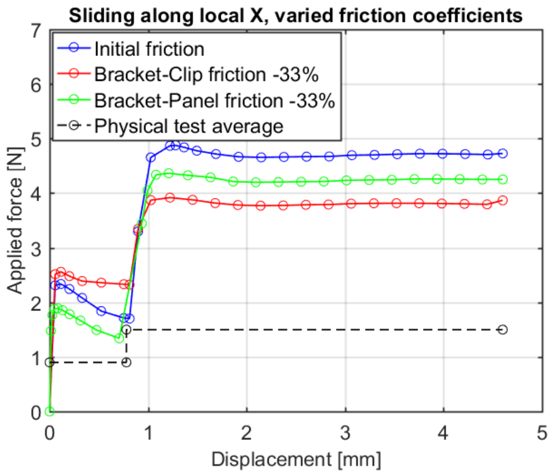

Figure 3.9: *Force required for sliding along local X. Initially chosen friction coefficients as well as varied friction coefficients compared to physical test average.*

The results show that when using the initial friction coefficients the two phases can clearly be seen by the increase in force as sliding between clip and bracket starts at approximately 0.8 mm displacement of the panel. However the force is overestimated as compared to physical measurements. When reducing the friction coefficient between panel and bracket it can be seen that the force is reduced for both phases. Moreover, when reducing the friction coefficient between clip and bracket there is an increase in force in the first phase and a decrease in force in the second phase. When the friction coefficient between clip and panel is reduced the two phase behaviour is not captured because the clip sticks to the bracket instead of sliding relative to it. This implies that the friction coefficient between clip and bracket should be greater than or approximately equal to the one between clip and panel.

Based on these results and iterations a set of friction coefficients for a final simulation were chosen in order to capture the two phase behaviour and a reasonable force magnitude as compared to physical tests. These friction coefficients compared to the initial values can be seen in Table 3.2.

Table 3.2: Suggested friction coefficients based on sensitivity study compared to initial values.

Interaction:	Initial μ:	Suggested μ:
Clip-Panel	0.30	0.10
Bracket-Panel	0.30	0.20
Clip-Bracket	0.31	0.11

The resulting force with the suggested friction coefficients compared to test average as well as range of spread between test specimens shown in grey can be seen in Figure 3.10. When using these values the ratio of the force between the first and second phase is approximately equal when comparing simulation result and test average. The spread between test specimens used in mechanical tests was $0.4 - 1.6$ N for sliding between clip and panel and $0.5 - 2.5$ N for sliding between clip and bracket [1]. Even though the force magnitude acquired from simulation with the suggested values is overestimated when compared to the physical test average it is still within this spread.

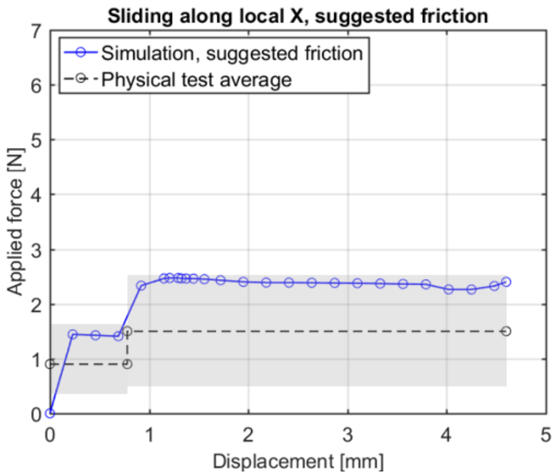

Figure 3.10: *Force required for sliding along local X. Suggested friction coefficients compared to physical tests. Range of spread between test specimens shown in grey.*

3.6 Torsional stiffness

The purpose of these analyses were to evaluate the torsional stiffnesses of the clip when the front sill moulding rotates relative to the bracket. In order to capture the behaviour of rotation around all three coordinate axes, three load cases were to be analyzed. Rotations were achieved by adding prescribed displacements to certain nodes of the front sill moulding. For a full description of the boundary conditions applied to the front sill moulding during all three rotations, see appendix B. The maximum rotational angles that were achieved during simulations and physical tests can be seen in Table 3.3. The aim was to achieve the same maximum rotational angle for simulations as in mechanical testing, however this was not possible for simulation of rotation around X since the clip is dis-assembled from the bracket at an angle of 18°. For simulation of rotation around Y the maximum angle could be reached, however further rotation would result in dis-assembly of the clip. For rotations around Z convergence issues were encountered at an angle of 28°. The simulated rotations at the maximum angle, as well as the positions where displacements were prescribed, are presented in Figures 3.11a, 3.11b and 3.11c.

Table 3.3: Maximum rotational angles in simulations and physical tests.

Load case:	Max angle, simulation:	Max angle, physical tests [1]:
Rotation around X	18° (0.31 *rad*)	25° (0.44 *rad*)
Rotation around Y	10° (0.17 *rad*)	10° (0.17 *rad*)
Rotation around Z	28° (0.49 *rad*)	30° (0.52 *rad*)

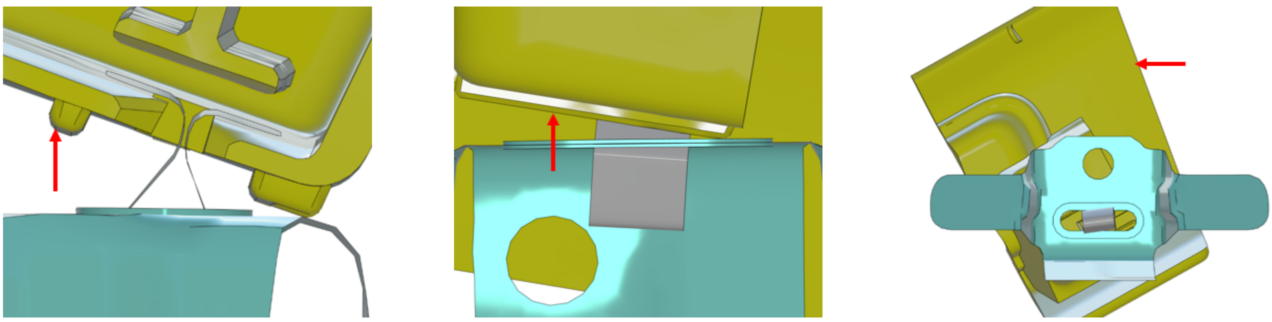

(a) *Rotation around X.* (b) *Rotation around Y.* (c) *Rotation around Z.*

Figure 3.11: *Maximum angles for the three load cases that were used to evaluate torsional stiffness of the clip.*

The force that was required to achieve rotation was obtained by extracting the total reaction force at the nodes where displacement was prescribed. This force was then used to calculate the torque by using the average torque arm which is defined as the distance from the center of the clip to the location where load is applied, as explained in Chapter 2.6.

The results from these analyses are highly dependent on the geometries between the different parts in the vicinity of the clip. This is of significant importance especially for rotations around X and Y since this aspect defines the point of rotation for these load cases. Since the interior panel used in mechanical tests is geometrically different as compared to the front sill moulding the behaviour in terms of torsional stiffnesses is not expected to be equal between the two different panels. Due to this fact, the test data are only used for comparison of simulation results. Furthermore the test data used for comparison are linear approximations of torque versus rotational angle between start and end of rotation for each load case.

3.6.1 Numerical results

One simulation for each rotation-analysis was run with the suggested parameters based on analysis of lateral stiffness and sliding along local X. The resulting torque versus rotational angle for rotations around X, Y and Z compared to the linear approximated data from physical testing can be seen in Figures 3.12a, 3.12b and 3.12c respectively.

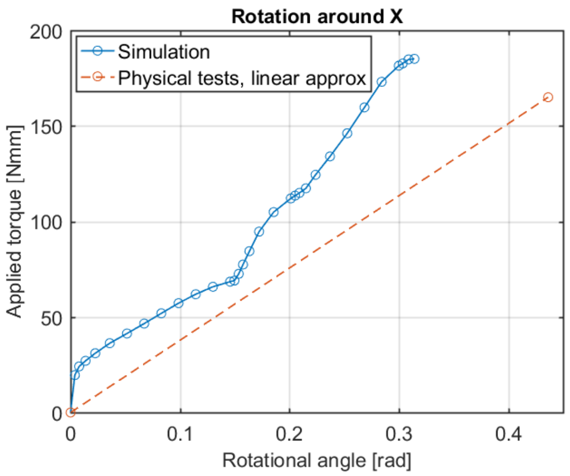

(a) *Rotation around X.*

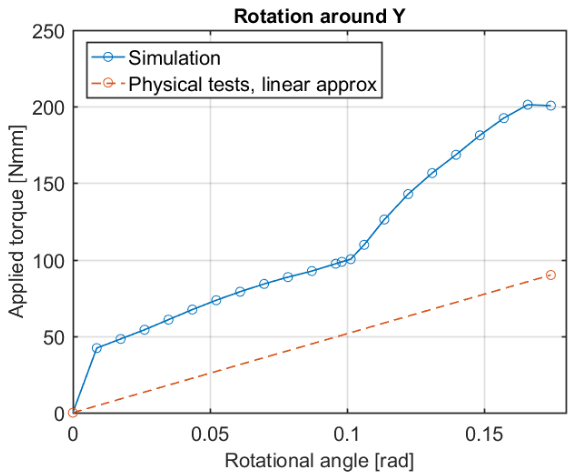

(b) *Rotation around Y.*

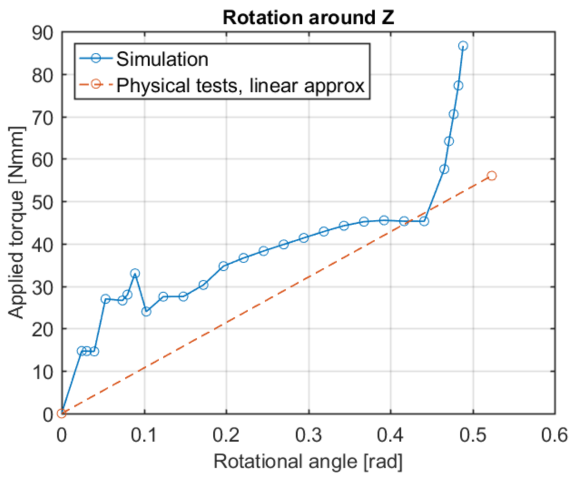

(c) *Rotation around Z.*

Figure 3.12: *Applied torque versus rotational angle for all three rotations. Simulation results and linear approximated physical test average.*

The torsional stiffness is initially very high for X and Y rotations, which is due to that a certain amount of torque is required in order to start rotation. After this initially high stiffness the slope is approximately constant until 0.15 rad for X-rotation and 0.10 rad for Y-rotation. At these angles the clip have been compressed and reached self contact which is why an increase in stiffness is seen. For X-rotation this stiffness is approximately constant until the end of the rotation and for Y-rotation constant until approximately 0.165 rad where the stiffness is reduced to zero until the end of rotation. The reason for the zero stiffness is that the clip rotates at this point instead of being compressed.

For Z-rotation an initially high stiffness is seen due to friction between the front sill moulding and bracket. At 0.10 rad the clip is compressed and the stiffness is approximately linear until it reaches self contact at 0.45 rad where an increase in stiffness is seen. The increased stiffness is approximately constant until the end of the rotation.

Based on the results acquired from the simulations the magnitude of torsional stiffness for varying rotational angles have been suggested for each rotation, see Table 3.4. The torsional stiffness presented in this table correspond to a piecewise linear approximation of the nonlinear behaviour observed in Figures 3.12a, 3.12b and 3.12c.

Table 3.4: Suggested torsional stiffness for varying rotational angles based on simulations.

Load case:	$\Delta\theta$ $[rad]$:	ΔM_a $[Nmm]$:	k_θ $[Nmm/rad]$:
X-rotation	$0.00 \rightarrow 0.15$	49.5	330
	$0.15 \rightarrow 0.31$	116.1	706
Y-rotation	$0.00 \rightarrow 0.10$	58.1	574
	$0.10 \rightarrow 0.17$	100.9	1562
Z-rotation	$0.00 \rightarrow 0.09$	33.0	369
	$0.09 \rightarrow 0.44$	21.3	60
	$0.44 \rightarrow 0.49$	41.3	873

3.7 Parameter study on torsional stiffness

To investigate how different parameters affect the results of these load cases a parameter study focused on contact properties was performed. In this analysis several simulations were carried out, each with one parameter altered compared to initial settings. The parameters that were chosen to alter and the magnitude of change can be seen in Table 3.5. For rotations around X and Y the friction coefficient between panel and bracket was assumed to have no effect on the torsional stiffness and thus is not included in the sensitivity analysis. Furthermore, the penalty stiffness factor is included in the sensitivity study. The reason for this is that the penalty stiffness factor was scaled in order for interference fit to converge, thus it is now scaled further to see the influence on the results.

Table 3.5: The parameters that were included in the parameter study and the magnitudes of variation compared to the initial magnitudes.

Parameter:	**X rotation:**	**Y rotation:**	**Z rotation:**	**Initial:**
Bracket-Clip friction	±50%	±50%	±50%	0.10
Panel-Clip friction	±50%	±50%	±50%	0.11
Bracket-Panel friction	-	-	±50%	0.2
Penalty stiffness factor	×0.1	×0.1	×0.1	×0.1

3.7.1 Numerical results

The resulting torque versus rotational angle for the parameter study of rotations around X, Y and Z compared to the initial simulation can be seen in Figures 3.13, 3.14 and 3.15 respectively.

The results show that an altered friction between bracket and clip has an effect for rotations around X and Y but not for rotations around Z. Friction between panel and clip has an effect for all three rotations, however the influence is decreasing as the rotational angle is increased. Friction between bracket and panel is the most influential parameter for rotation around Z, which is due to the normal forces that arise due to the gravity load of the panel.

A scaled penalty stiffness does not have a large effect on rotations around Y. For rotations around X it does not have a significant effect until the maximum angle where the reduced penalty stiffness causes earlier dis-attachment of the clip. For rotations around Z a reduced penalty stiffness results in a missed peak torque at approximately 0.08 *rad*.

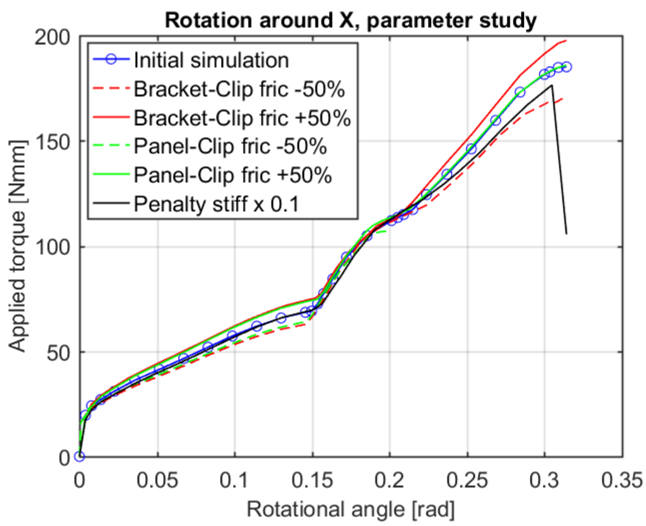

Figure 3.13: *Results from parameter study of rotation around X.*

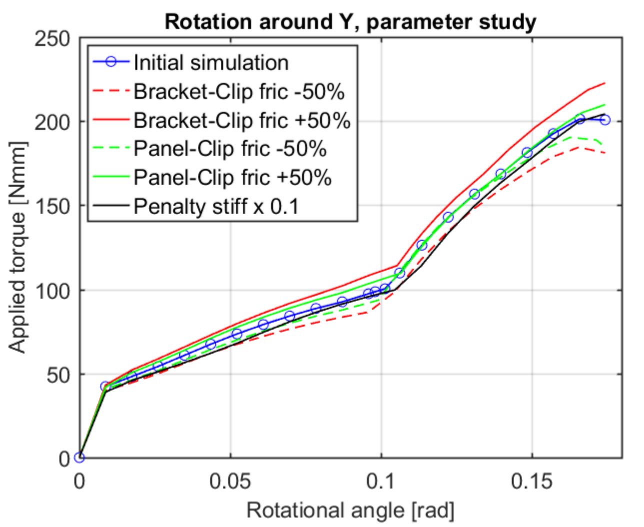

Figure 3.14: *Results from parameter study of rotation around Y.*

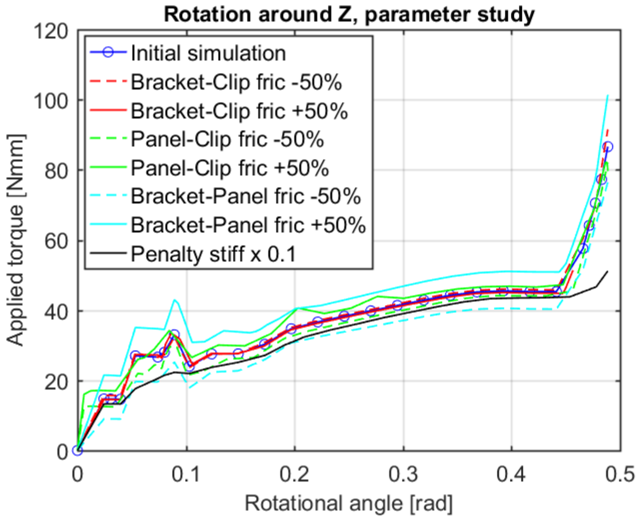

Figure 3.15: *Results from parameter study of rotation around Z.*

4 Evaluation of force for assembly and disassembly

In this chapter previous work related to mounting and dismounting of the front sill moulding is explained. Then the methodology used to numerically predict the forces required for assembly and disassembly is explained and lastly the results from simulations are presented.

4.1 Previous work

At Volvo Cars physical measurements have been performed to evaluate the force contribution from clips when the front sill moulding is mounted to the car body. For the purpose of these measurements a plate with the same thickness as the brackets was used, see Figure 4.1a. The plate has four holes with different widths, the first one being the same as the one in the brackets, i.e. 5.2 mm, and the three other holes have a width of 5.4, 5.5 and 5.6 mm respectively. During these measurements a part of the front sill moulding, as well as the aluminum insert were included, see Figure 4.1b. In order to isolate the force contribution to only the clip the guiding pin that in reality is located beside the clip was excluded. The assembly force was measured using a dynamometer with a diameter of 10 mm and the load was applied right above the center of the clip. During measurements the aim was to keep the top of the panel at a horizontal position and this was assured by holding the aluminum insert by hand [10]. The maximum assembly forces were recorded for four clip specimens for each hole width and the average values for each respective hole width are used for correlation of simulations.

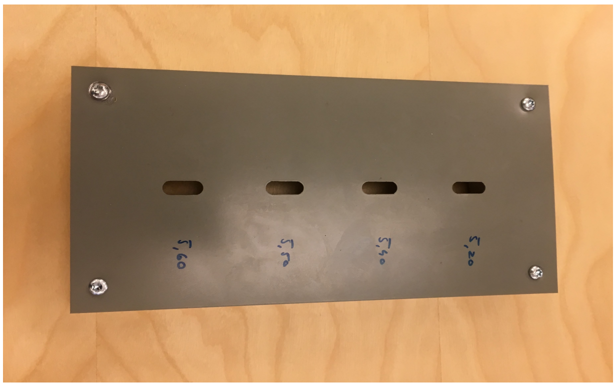

(a) *The steel plate with four holes of varying sizes.*

(b) *The part of the front sill moulding and the aluminum insert during assembly.*

Figure 4.1: *Parts used during testing. Figures produced with permission from [10].*

In addition to the tests described above measurements have been performed for mounting of the complete front sill moulding [16]. However the mounting of complete panels involves a lot of aspects that contributes to the assembly force beside the clips. These aspects include influence from guiding pins, sealing, tolerances and base carpet. Without including all these aspects in the simulation model correlation to these measurement data is difficult. However, by comparing these data it is possible to make an estimation of what fraction of the force the clips contribute to during the real assembly process.

No physical tests for the disassembly force of the front sill moulding have been performed at Volvo Cars. However, the manufacturer of the clip has suggested a maximum value for which the clip contributes to the force required for disassembly [4]. This value is used for correlation of simulations regarding disassembly.

4.2 Methodology

The methodology used to predict the forces required for assembly and disassembly of panels was to first develop an FE-model based on the measurements performed on a plate with four different holes. This FE-model is then calibrated to give a reasonable behaviour for a hole size of 5.2 mm since this is the actual hole size used in vehicles. After reasonable results where achieved for this hole size assembly with the other three hole sizes where simulated. A parameter study is then performed on the assembly process where friction coefficient between clip and plate as well as velocity are varied. After this disassembly is simulated for 5.2 mm hole size since measurement data is only available for this size. Lastly a scaled up FE-model including the complete front sill moulding and the brackets used in vehicles is developed. This model is used to evaluate the clips contribution to the assembly force during actual conditions. An overview of the methodology used for this part of the project can be seen in Figure 4.2.

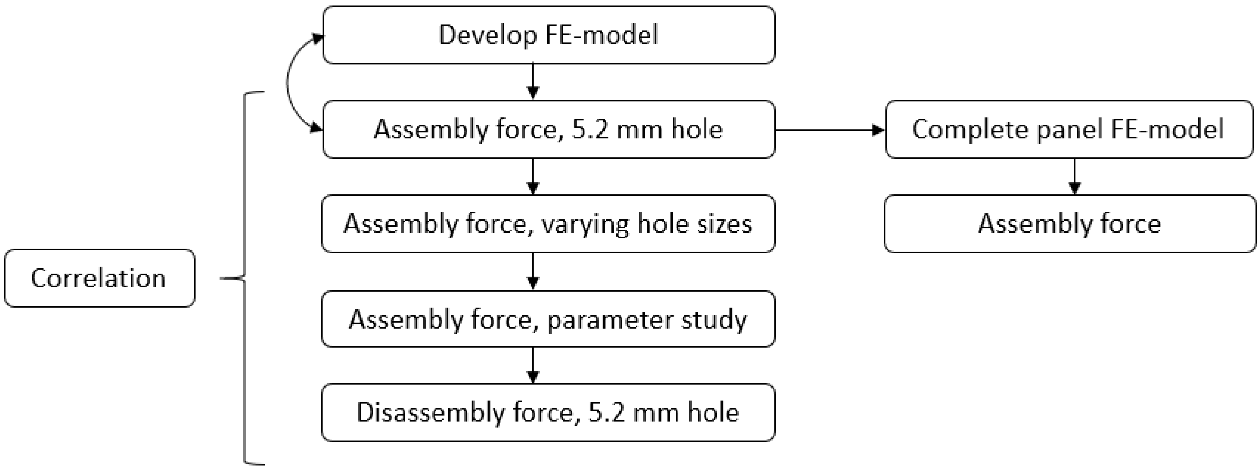

Figure 4.2: *The methodology used to evaluate assembly and disassembly force.*

4.2.1 Post processing of results

Since the assembly process is associated with a lot of interaction between parts and snap-through as the clip waist passes the plate a dynamic analysis with explicit time integration was chosen for this part of the project. The solution procedure for this analysis type is described in Appendix A. Since the results from a dynamic explicit analysis contains noise, force history during assembly and disassembly is hard to distinguish when comparing multiple results in the same plot. For the purpose of being able to compare results a channel frequency class (CFC) 60 filter is used which gives a smoother curve. This filter does not always capture maximum values, it should rather be seen as an approximation of the unfiltered results which makes it easier to distinguish the behaviour of assembly and disassembly. Since maximum values are not always captured when using this filter the maximum values presented in the upcoming chapter is based on the unfiltered results. However, when comparing force history between multiple simulations the filtered results are always used.

Furthermore, all results related to assembly force presented in this chapter have been normalized by the maximum acquired force during physical testing of the plate with four holes. The results related to disassembly force have been normalized by the disassembly force suggested from the manufacturer of the clip. The reason for this is to meet Volvo confidentiality requirements.

4.3 FE-model setup

For the purpose of simulating assembly and disassembly a FE-model based on the geometries of the parts used during measurements was developed, see Figure 4.3. The element types that are used for the mesh are reduced integration shell elements, denoted S4R and S3R in Abaqus. Computational efficiency may be increased by using this type of elements as compared to conventional shell elements, however caution should be taken since unphysical behaviour such as hourglass effects may be observed as discussed in chapter 29.6.2 in [5]. In this model hourglass effects are checked by looking at the artificial strain energy during the analysis, see Appendix C. The target element sizes used for the different parts were 1 mm for the clip, 3 mm for the panel and 2 mm for the plate. Furthermore the elements of the panel were refined around the area where the clip is located thus resulting in an element size of 2 mm in this particular area.

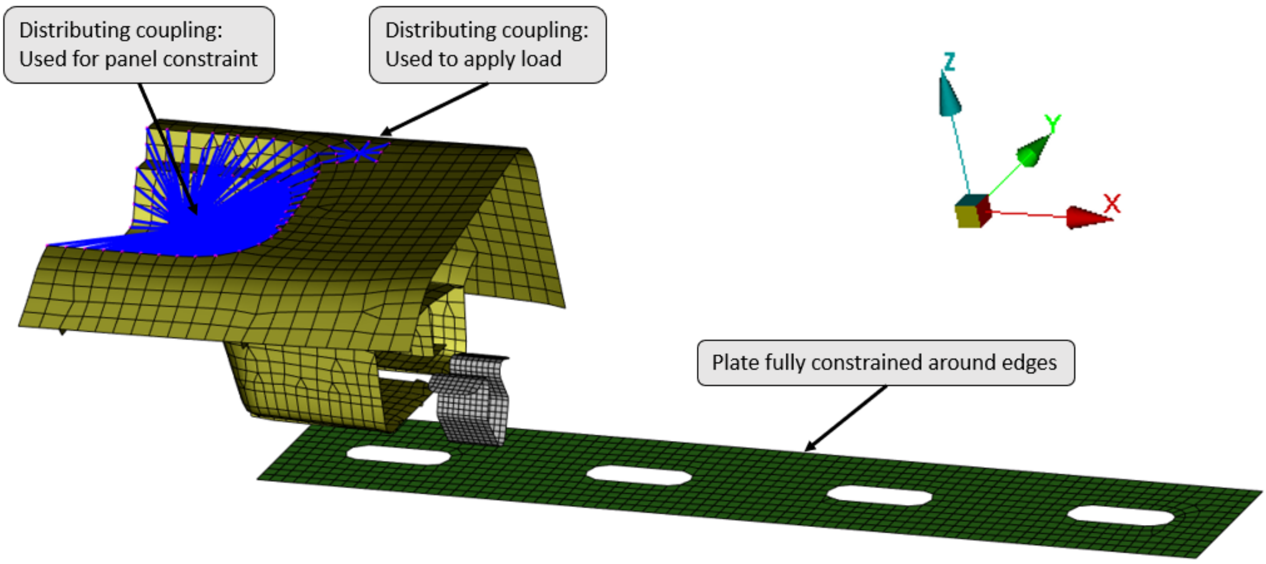

Figure 4.3: *The FE-model used to evaluate assembly and disassembly force and the nodes used for boundary conditions.*

In this analysis the clip material was approximated as linear elastic with a Young's modulus of 201 GPa. The reason for this is that when using elastoplastic material data large plastic deformations for the clip were observed after simulation of assembly process. These deformations do not correspond to what is seen in reality.

As friction coefficients the suggested values from correlation of sliding capability of the clip were used, see Table 3.1 in Chapter 3.3. The panel was constrained from movement in DOF u_x, q_x and q_y. When constraining the panel from movement in DOF u_y and q_z it was noticed that the reaction forces in the constrained nodes were very high which gave rise to large unphysical peaks in assembly force. This problem was solved by instead adding a connector element with elastic spring properties for translation in DOF u_y and q_z. This set of boundary conditions allows the clip to position itself and ensures that the top of the panel is horizontal. The plate was constrained from movement in all directions at the edge-nodes. All constraints and the boundary conditions used for assembly and disassembly where specified as velocity. The nodes included in the distributing coupling used to apply the assembly-load forms a circle with an approximate diameter of 10 mm, thus replicating the size of the dynamometer used during mechanical testing of assembly force.

4.4 Assembly force

Before assembly of the front sill moulding onto the plate could be simulated, the clip had to be assembled onto the front sill moulding. This was done by applying a prescribed velocity to the clip while fully constraining the front sill moulding from movement as an initial simulation step. After this, a velocity of 27.4 mm/s was applied to the distributing coupling node located above the clip until assembly of the front sill moulding onto the plate was completed. The simulation steps can be seen in Figures 4.4a, 4.4b and 4.4c.

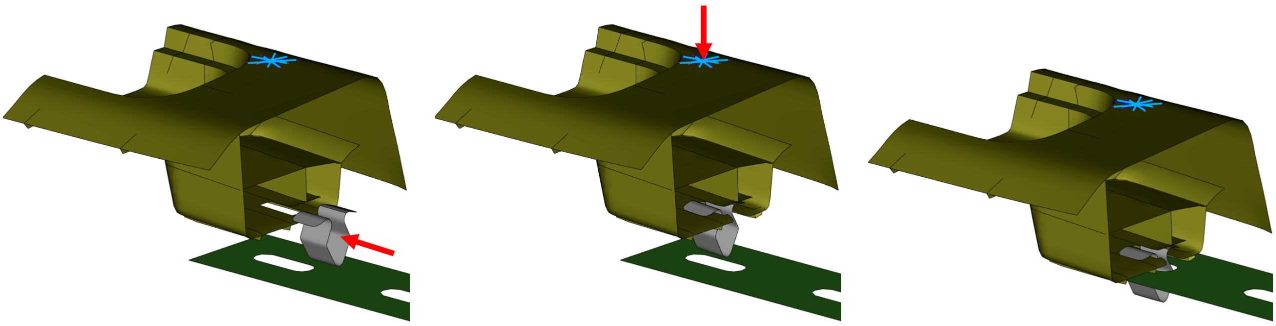

(a) *The clip is assembled onto the front sill moulding.* (b) *The front sill moulding is assembled onto the plate.* (c) *End of assembly.*

Figure 4.4: *Assembly simulation steps.*

4.4.1 Numerical results

The resulting assembly force for the 5.2 mm hole width, filtered and unfiltered values, can be seen in Figure 4.5. The figure show that the assembly have two force peaks, the first one at approximately 2.5 mm displacement and the second one approximately at 4.5 mm. The position of the clip during these force peaks can be seen in Figures 4.6a and 4.6b respectively.

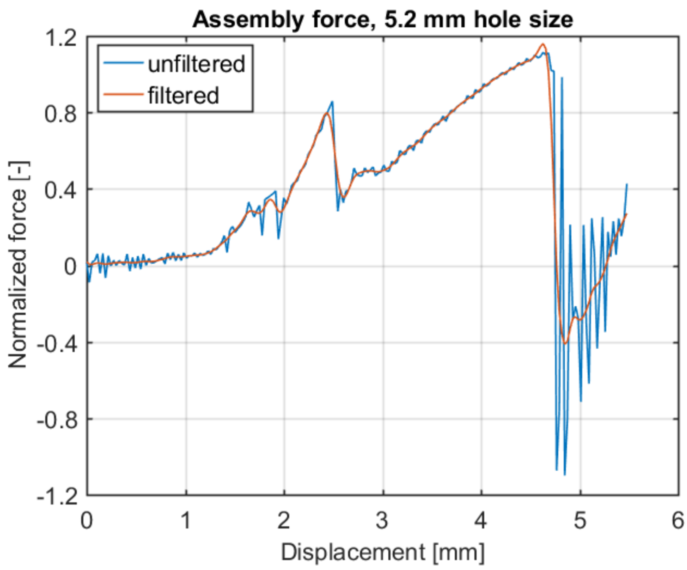

Figure 4.5: *Force required for assembly with 5.2 mm hole width when using friction coefficients found from correlation of sliding capability. Actual and filtered assembly force normalized by the maximum measured assembly force during physical tests.*

The reason for the first force peak is due to sticking friction between the interacting surfaces. Up to this point, the shear stresses between the surfaces in contact are lower than the threshold value for sliding thus resulting in compression of the clip in Z-direction. When the critical shear stress is reached, sliding starts and as a consequence a sudden drop in force is seen. The reason for the second force peak is due to the clip waist being wider than the hole when the gap of the clip has been closed, see Figure 2.4a in Chapter 2.6. The assembly force increases until the waist of the clip has been compressed enough to pass the hole. After this assembly is complete and a drop in force is seen when the built up strains in the clip are released. At approximately 4.8 mm displacement, the panel is in contact with the plate which is why an increase in assembly force is seen.

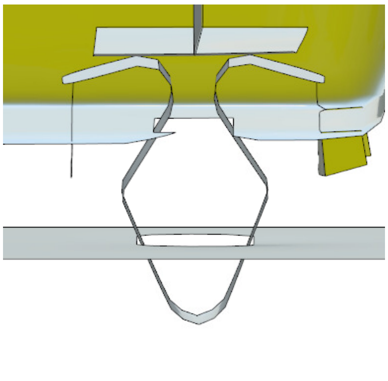

(a) *Clip position at the first force peak.*

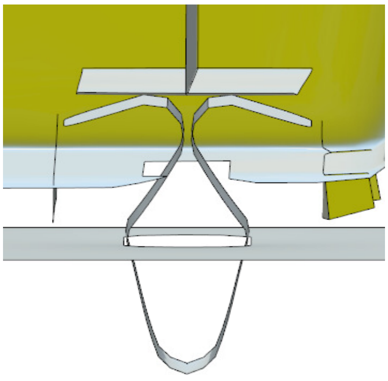

(b) *Clip position at the second force peak.*

Figure 4.6: *Clip position at the two force peaks during assembly for 5.2 mm hole width.*

The effects of varying hole widths can be seen in Figure 4.7a. As can be seen the second peak in force is reduced with increased hole width. The reason for this is that the clip does not have to be compressed as much laterally before the assembly is finished. However for the first peak the effects of increased hole width is not as clear. The magnitude of the first peak is largest for 5.2 mm and then 5.5 and 5.6 mm. For a hole width of 5.4 mm the peak is not visible. The reason for this may be that this peak is not only dependent on the sticking friction but also on how the clip positions itself in the hole.

In Figure 4.7b the maximum unfiltered force acquired from simulations are compared to the maximum measured values. When comparing the maximum force from simulations to the measured results it can be seen that the force is overestimated for hole sizes 5.2, 5.4 and 5.6 mm. However, the behaviour in terms of increased force for a hole size of 5.5 mm is captured.

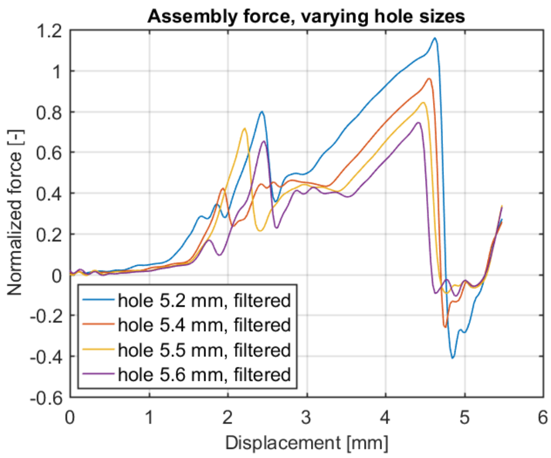

(a) *Assembly force for different hole widths. Filtered results.*

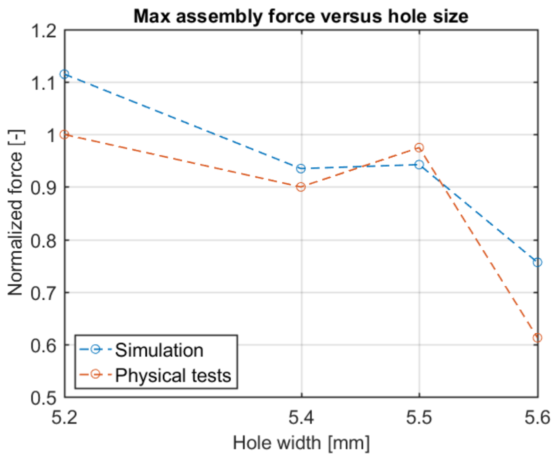

(b) *Maximum force for varying hole sizes from simulations compared to physical tests. Simulation values are based on the unfiltered results.*

Figure 4.7: *Assembly force for varying hole widths. Filtered force history and maximum values from unfiltered results normalized by the maximum value from physical tests.*

The maximum assembly force decreases approximately linearly, except for 5.5 mm hole size, hence this result is investigated more in detail. The resulting force history for this hole size can be seen in Figure 4.8. When looking at the unfiltered results the maximum force occur at the first peak in contrast to the other hole sizes, where the maximum force occur at the second peak.

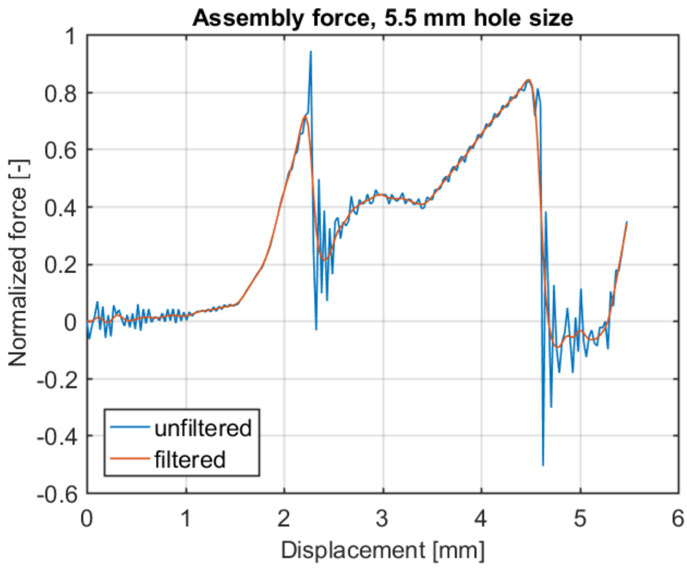

Figure 4.8: *Force required for assembly with 5.5 mm hole width. Unfiltered and filtered results.*

4.5 Parameter study of assembly force

Since the maximum force acquired from simulations were overestimated for three of the hole sizes the effect of a reduced friction coefficient between the clip and the plate were further investigated. The resulting force history for a hole size of 5.2 mm and reduced friction can be seen in Figure 4.9a. The effect of a reduced friction coefficient was evaluated for the other hole sizes as well and the maximum force from the unfiltered results can be seen in Figure 4.9b. With a reduced friction coefficient between the plate and the clip the maximum force correspond better with physically measured data for hole sizes 5.2, 5.4 and 5.6 mm. However the increase in force for hole size 5.5 mm is not captured with reduced friction.

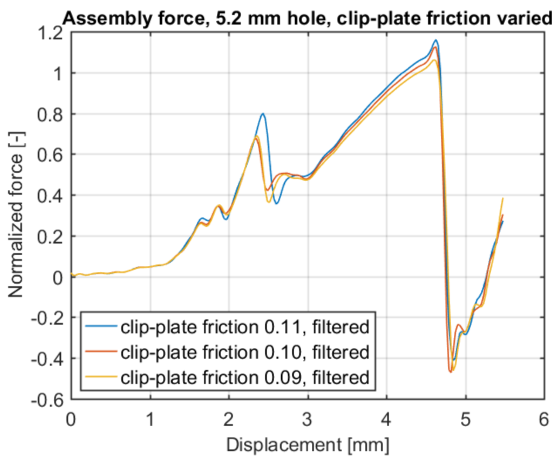

(a) *Assembly force for hole size 5.2 mm and reduced friction coefficient between clip and plate. Filtered results.*

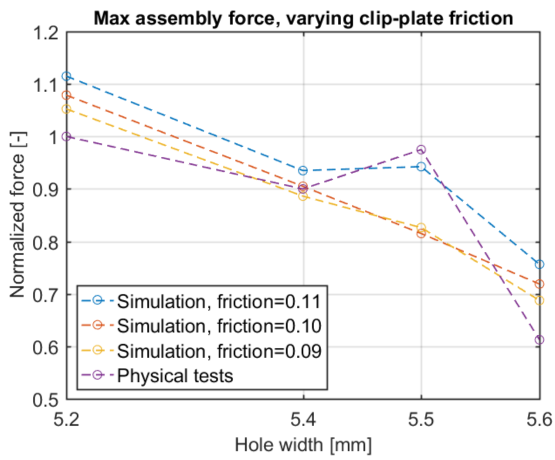

(b) *Maximum assembly force for all hole sizes and reduced friction coefficient between clip and plate.*

Figure 4.9: *Assembly force, varying hole widths. Force history and maximum values.*

The influence of the velocity during assembly was investigated by running two simulations, the first one with a reduced velocity of 50 % and the second one with an increased velocity of 50 %. The filtered results can be seen in Figure 4.10 for a hole size of 5.2 mm. The results show that when altering the velocity the first peak force is not captured as clearly as it is when using initial conditions. However, the second peak force is not affected.

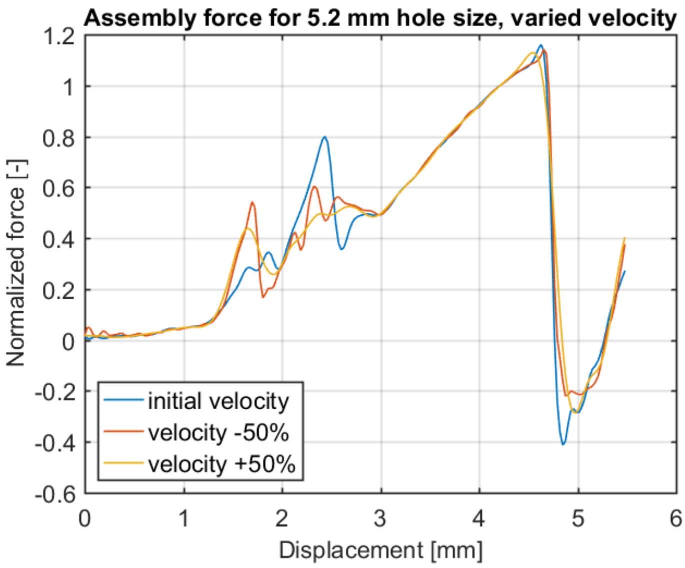

Figure 4.10: *Effects of varying assembly velocity.*

In summary, the parameter study regarding effects of varied clip-plate friction coefficient and assembly velocity show that the first force peak is highly sensitive to both studied parameters. It should be mentioned that when discussing the test data that are used for correlation with the engineers who conducted the tests, there were some uncertainties regarding the validity of the measured force for a 5.5 mm hole width. Due to the unexpected increase in force as compared to a 5.4 mm hole width the impression was that either errors had been made during measurements or that the 5.5 mm hole was erroneously created. Furthermore, since only the maximum assembly forces were measured it is difficult to establish the validity of the simulation results acquired related to the first force peak. In order to establish the validity, more tests have to be conducted where the force history is measured such that the point where maximum assembly force in reality occur can be determined.

4.6 disassembly force

The force required for disassembly was evaluated starting from the assembled state described in the previous section. Data available for correlation of this process is only available for a hole size of 5.2 mm. Since the friction coefficients found from correlation of sliding capability resulted in reasonable correlation during assembly these were used for the disassembly process as well. The velocity corresponding to the disassembly load was applied at the same area that the velocity for assembly was applied to.

The material for the clip was again approximated as linear elastic steel, however during simulation this approximation resulted in an unsuccessful disassembly. Instead the area of the front sill moulding in the vicinity of the clip experienced plastic deformation and the clip was disassembled from the front sill moulding instead of the clip. The reason for this is that during disassembly the angle of the clip where it is in contact with the plate is too large, see Figure 2.4b in Chapter 2.6, thus yielding a normal force for which the composant in lateral direction is too small to result in compression of the clip waist. The resistance provided from the linear elastic steel is too large and consequently the front sill moulding is deformed instead of the clip. The reason why this approximation give good correlation for assembly but not for disassembly is that the composant in lateral direction for the clip is larger during assembly thus resulting in a larger force that contributes to compression of the clip waist.

In order to be able to get an estimation of the force required for disassembly the material of the front sill moulding was artificially stiffened by increasing the Young's modulus. When using this approximation disassembly was successful, however the results show that instead the plate experienced plastic deformation. In Figure 4.11a the resulting force during assembly can be seen. The maximum force is approximately four times the value suggested from the manufacturer of the clip and thus highly overestimated.

When instead using elastoplastic material data for the clip the resulting force was highly underestimated as compared to suggested value from the manufacturer of the clip, see Figure 4.11b. This is due to the large residual deformation of the clip that is present after the assembly process.

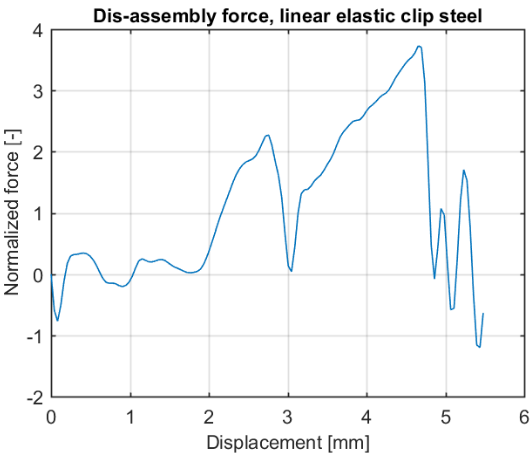

(a) *disassembly force when using linear elastic clip steel and an artificially stiffened panel.*

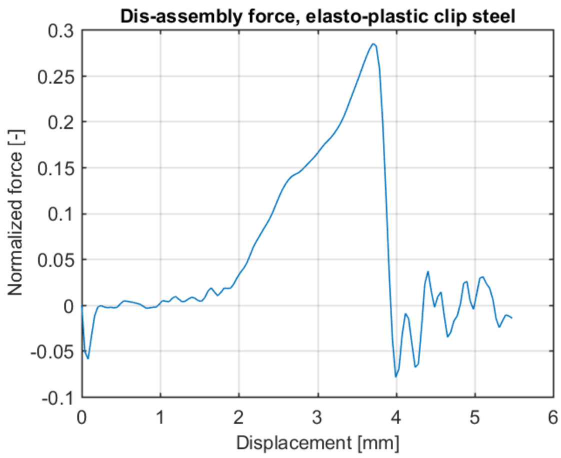

(b) *disassembly force when using elastoplastic clip steel.*

Figure 4.11: *Force required for disassembly normalized by the value suggested from the manufacturer of the clip. Linear elastic clip steel with an artificially stiffened panel and elastoplastic clip steel respectively.*

4.7 Assembly force of complete panel

In order to evaluate the assembly force when including the complete front sill moulding a FE-model was developed where a large part of the car body, three brackets, three clips and the complete front sill moulding except for the guiding pins were included. The parts as well as the boundary conditions applied to the car body can be seen in Figure 4.12. The element types that are used for all parts are reduced integration shell elements, denoted S4R and S3R in Abaqus [5]. The brackets were connected to the car body by use of connector type beams which resemble the spot welds that in reality connect these parts. The clip connections are mounted one by one starting with the left one and ending with the right one as shown in Figure 4.12.

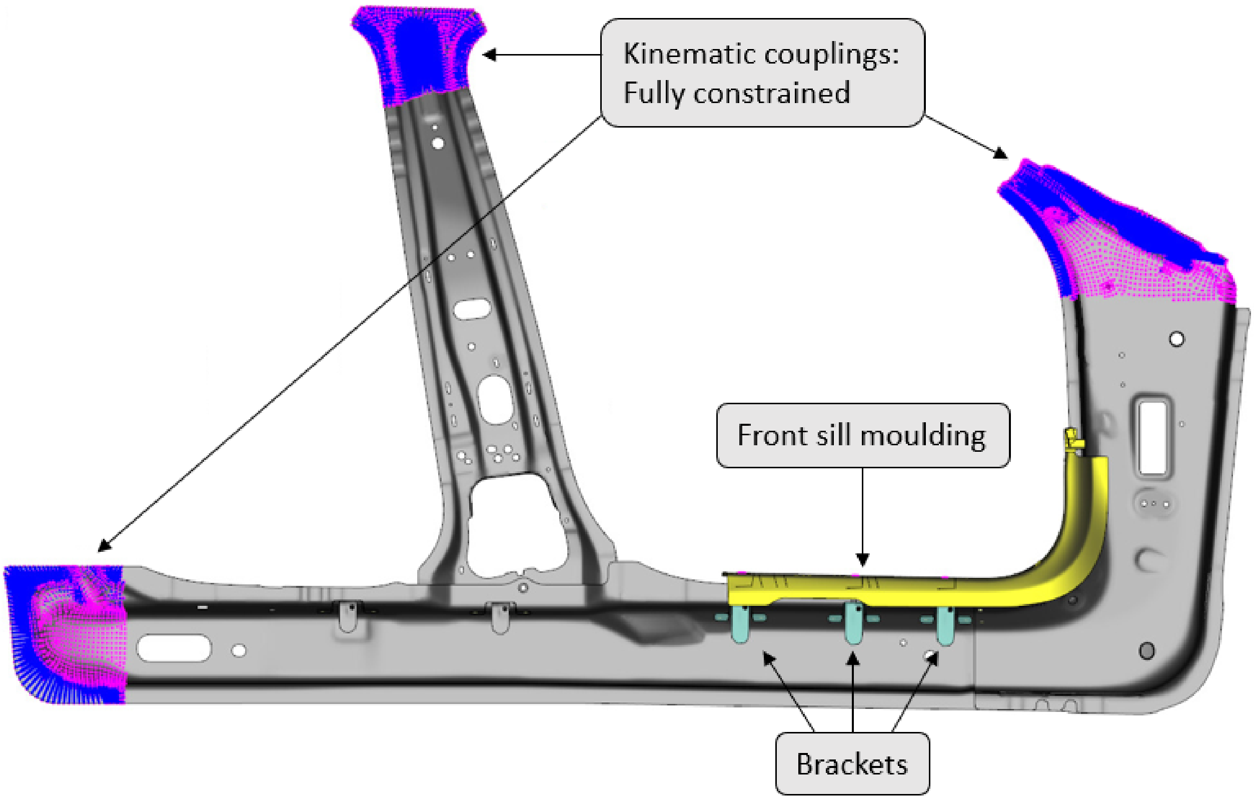

Figure 4.12: *FE-model used to evaluate the assembly force when including the complete front sill moulding. The boundary conditions for the car body as well as the order of assembly is shown.*

The purpose of this analysis was to evaluate the force contribution from the clips in more realistic conditions. The assembly process of the complete panel was simulated by applying a velocity of $27.4m/s$ located right above the clip in a similar manner as for the FE-model described in chapter 4.3. Figure 4.13a show where the load was applied for the first clip connection, the load was applied in the same way for the two other clip connections. The guiding pins have been excluded in this FE-model as well, however the guiding that the pins provide have been kept. This was done by constraining the nodes where the load is applied in all DOF's except u_z. The reason for doing this is that in reality the guiding pins determine how the clips are positioned in the hole, thus resulting in a more realistic simulation. In Figure 4.13b the assembled state of the first clip connection can be seen.

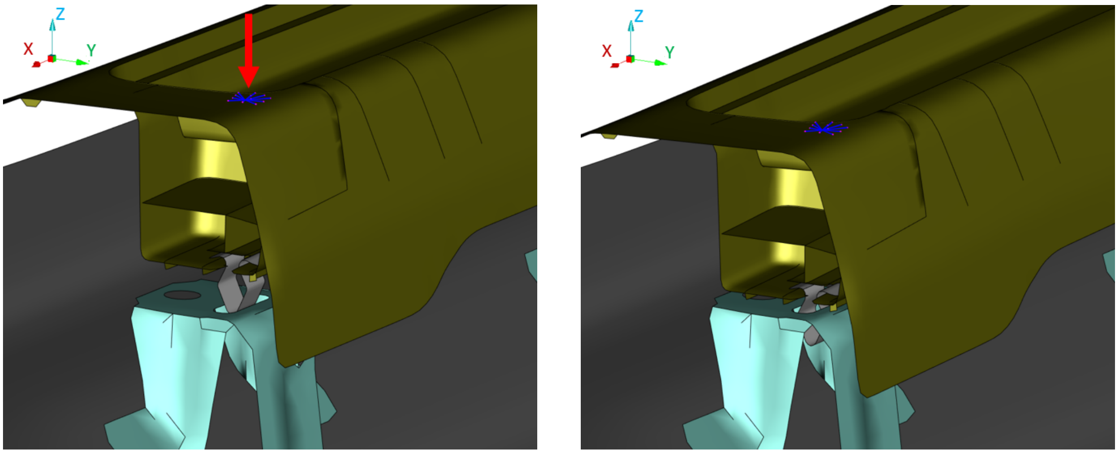

(a) *The first clip connection and area where the load is applied.*

(b) *The first clip connection after completed assembly.*

Figure 4.13: *The first clip connection before and after assembly.*

4.7.1 Numerical results

The assembly force for the first clip connection can be seen in Figure 4.14. The behaviour is similar to the assembly force acquired when only including a part of the front sill moulding and the plate, see Figure 4.5 in Chapter 4.4. The maximum force measured during previously performed tests including the complete front sill moulding suggests an average normalized assembly force of 4.4 for the first clip connection [16]. Based on the maximum force acquired from the simulation, it can be concluded that the contribution by the clip is approximately 1/4 of the total force.

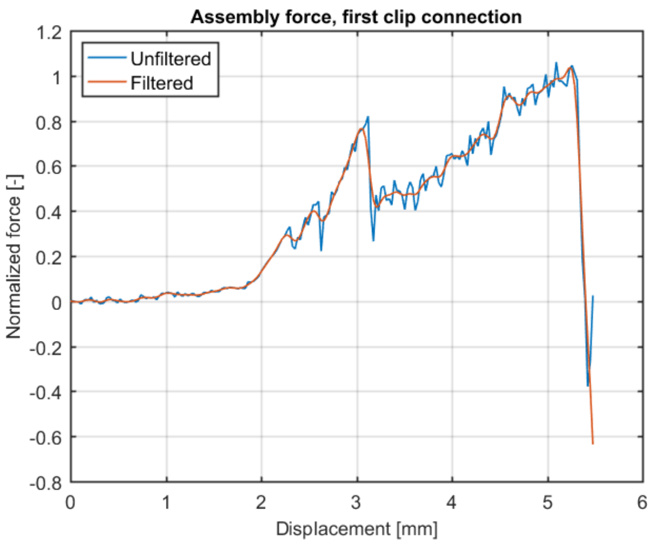

Figure 4.14: *Assembly force for the first clip connection when including the complete panel. Unfiltered and filtered curves.*

For the second and third clip connections the resulting assembly force was hard to distinguish due to highly fluctuating noise. Further development of the FE-model is recommended in order to acquire trustworthy results for these clip connections.

5 Discussion

5.1 Mechanical properties of the clip

The clip specimens used during mechanical testing of lateral stiffness previously performed at Volvo Cars had an average gap size of 2.87 mm and a spread between 2.5 and 3.1 mm [1]. The reason for the variation in gap size between clip specimens is unknown. Two possible reasons for this are that some of the clips may have already been subjected to loads before measurements were conducted and that variations in geometries arise due to tolerance specifications during manufacturing. Furthermore, the nominal gap-size of the CAD-model used for the FE-model is 3.3 mm. When implementing two simulation steps where the clip is first compressed and then released a gap-size within the range of spread for the test specimens was achieved. However, due to the mentioned uncertainties, it is difficult to judge if this behaviour is seen in reality.

The measurements related to sliding capability that were previously conducted at Volvo Cars consisted of ten clip specimens, which yielded a wide spread in results [1]. The estimated average used for correlation of simulation results is thus only a fictional value, however it provides some indication of what results to aim for. Whether the spread in test results depends on errors made in measurements, geometrical differences between test specimens or other deviating material properties is difficult to establish. Furthermore, during measurements the panel was displaced 10 mm which can be compared to the sliding distance of 4.6 mm that was implemented during simulations. The reason for the distance being lower in simulations is that the clip at start of sliding is in the center position of panel and bracket. Simulations were carried out where the panel was first displaced to one side in one step and then to the other side in the next step to be able to slide the full distance. Due to convergence issues no results could be acquired from these simulations. However, since the behavior of sliding between clip-panel and clip-bracket is captured with an approximately constant force during both phases, this sliding distance is considered sufficient for a comparison with test results.

There is a difference between the part of panel that was used for mechanical testing of the torsional stiffnesses of the clip and the one that was used for the FE-model. The geometry of the panel is crucial when simulating rotation around X and Y since it defines where the panel hits the bracket while rotating. Because of this aspect the torsional stiffnesses that have been presented are not valid for just the clip, but rather representative for the structure in the vicinity of the clip.

5.2 Assembly and disassembly

When simulating the assembly process, the boundary conditions that are used to constrain the panel from movement are very important to consider. It was noticed that when constraining the panel from movement in all degrees of freedom except for the direction of assembly, large reaction forces in the constrained nodes arise. The reason for this was that the panel was not exactly aligned so that the clip is perfectly aligned with the hole. During simulations this problem was solved by adding springs so that some translation in Y-direction and rotation around Z were allowed for the panel. The stiffnesses of these springs were chosen based on the reaction forces that were observed when instead using fixed constraints. This results in a positioning of the clip during simulation which is more accurate in terms of capturing the conditions during physical tests.

When using elastoplastic material data for the clip large residual deformations were present after assembly simulation. The clip is highly compressed and due to this no resistance is provided in the assembled state in terms of normal force between clip-plate and clip-panel. The reason for this is possibly that in reality there are unknown residual stresses in the material of the clip as well as an increased yield limit due to bending during manufacturing of the clip. In an attempt to avoid the residual deformation present after assembly the same approach used when setting up the FE-model for evaluation of mechanical properties was tested. Instead of performing assembly an implicit analysis step was added before disassembly where interference fit was performed. However, no converged solution was obtained. Furthermore, another approach was tested where the elements closest to the lower bent area of the clip was modelled as linear elastic steel while the elements of the rest of the clip was modelled as elastoplastic. This resulted in unsuccessful disassembly just as for the case where the clip was fully modelled as linear elastic.

6 Conclusions

6.1 Mechanical properties of the clip

This thesis provides Volvo Cars with a method to predict the mechanical properties of the studied clip in terms of sliding capability and lateral and torsional stiffnesses during relative movement between the front sill moulding and the bracket.

The results acquired from simulations may be used to calibrate a connector element that represent the clip to be used in simulations involving the front sill moulding. However, some of the evaluated properties are highly dependent on the geometries of the surrounding parts and thus not representative for only the clip. This is especially true for the torsional stiffnesses for rotations around X and Y where the point of rotation between front sill moulding and bracket is defined by the geometries in the vicinity of the clip. Furthermore, the simulation results for sliding along local X as well as torsional stiffness for rotation around Z includes influence from frictional forces between the front sill moulding and the bracket. Because of this, it is recommended to exclude friction between the interacting surfaces if a connector element representation is to be implemented based on the simulation results.

6.1.1 Future work

In order to find properties that are more general to the clip, rather than the complete structure, it is recommended to find a way to isolate the influence to the clip only. If this is successfully done, it would be possible to calibrate a more general connector element that can be applied to other plastic components attached by this type of clip.

The simulations performed for evaluation of mechanical properties of the clip have been carried out with material data for room temperature. Since temperatures in the vicinity of the studied area of the vehicle can reach temperatures up to 80°C it is recommended to run the simulation model for this temperature as well to see the influence of an increased temperature.

6.2 Assembly and disassembly

The simulation work of this thesis provides Volvo Cars with a method to predict the assembly force contribution of the studied clip. This method may be used to test parameters such as how a change in geometry of the clip would affect the assembly force. Furthermore this thesis provides an understanding of the behaviour of the clip during the assembly process which may be used in future development related to improvement of the ergonomic aspects of this process.

The set of friction coefficients between parts found from correlation of sliding capability yielded a resulting assembly-force that correlate well to physical tests performed for varying hole sizes. However due to uncertainties expressed by the engineers that conducted the tests, further validation is needed in order to establish the validity of this set of friction coefficients.

The results related to the assembly process show that there are two peaks in assembly force. The first one due to sticking friction between the clip and the other parts and the second one highly dependent on the waist of the clip when being compressed laterally. When increasing the size of the hole the effects on the assembly force would be the same as altering the geometry of the clip so that the width of the waist is reduced when the clip is compressed. Consequently, as the results show, this force peak is reduced with increasing hole size. The conclusion that can be drawn from this result is that a reduced waist of the clip would result in a lower second peak. However, the magnitude of the first force peak does not have a clear relation to the hole width. As was shown in the parameter study, this force peak is highly sensitive to variations of both friction between clip and plate as well as velocity of assembly. Further validation is needed to establish the validity of the results related to this force peak.

The resulting force acquired from simulation of assembly of the first clip connection when including the complete front sill moulding is similar to the force when only including a part of the panel. This result implies that a simplified method is sufficient in order to capture the force contribution from the clip for the first clip connection. For the two other clip connections the stiffness of the panel is assumed to have a larger effect.

6.2.1 Future work

The physical test data that are available for correlation does only include the maximum values of force during assembly. To further validate the simulation results it is recommended to perform tests where the complete force history is measured during assembly. This would enable correlation of both force peaks observed from simulations. Furthermore, since uncertainties of the test equipment as well as the measuring methods were expressed, it is recommended to carry out more extensive tests to ensure the validity of the results. For example, if five identical plates had been used instead of one it would have been possible to identify equipment defects such as imperfect holes.

When simulating disassembly the force was highly overestimated when using linear elastic steel and highly underestimated when using elastoplastic steel for the clip. As previously discussed the change in material properties that occur due to the manufacturing process of the clip have not been taken into account during this project. A conclusion that can be drawn from these results is however that it is recommended to model these properties of the clip in order to be able to get an accurate estimation of the disassembly force. This would result in a stiffness that is somewhere in between the two material approximations used in this analysis. An other method of solving this issue may be to solve the convergence issues that arise when interference fit was performed. This would allow for a disassembly starting from an undeformed state of the clip, but still using elastoplastic material data.

When simulating assembly for the complete panel the resulting force for the two last clip connections was unidentifiable due to highly fluctuating noise. It is recommended to investigate other possible boundary conditions of the panel in order to solve this issue.

References

[1] K. Behbahani. *Clips in strength analysis - Measurement of sliding forces.* Internal document at Volvo Car Corporation, Gothenburg, July 8, 2016.

[2] BETA CAE Systems. *ANSA, Version 17.1.3, Accessed April 23, 2018.* https://www.beta-cae.com/.

[3] BETA CAE Systems. *META, Version 17.1.3, Accessed April 23, 2018.* https://www.beta-cae.com/.

[4] A. G. Co.KG. *AR-NR. 247410-X Development versions, [Unpublished report].*

[5] Dassault Systèmes. *Abaqus Analysis User's Guide, Version 6.14, Accessed April 23, 2018.* https://www.3ds.com.

[6] Dassault Systèmes. *Abaqus Theory Guide, Version 6.14, Accessed April 23, 2018.* https://www.3ds.com.

[7] Dassault Systèmes. *Abaqus/Explicit, Version 2017, Accessed April 23, 2018.* https://www.3ds.com.

[8] Dassault Systèmes. *Abaqus/Standard, Version 2017, Accessed April 23, 2018.* https://www.3ds.com.

[9] F. Harewood and P. McHugh. Comparison of the implicit and explicit finite element methods using crystal plasticity. *Computational Materials Science* **39**.2 (2007), 481–494. ISSN: 0927-0256. DOI: https://doi.org/10.1016/j.commatsci.2006.08.002. URL: http://www.sciencedirect.com/science/article/pii/S0927025606002278.

[10] S. Helmroth. *Personal communication.* Gothenburg, April 26, 2018.

[11] F. Larsson. *Non-linear finite element analysis.* Department of Applied Mechanics, Chalmers University of Technology, 2010.

[12] Mathworks. *MATLAB, Version R2016B, Accessed April 23, 2018.* https://se.mathworks.com/products/matlab.html.

[13] N. Saabye Ottosen and H. Petersson. *Introduction to the finite element method.* New York: Prentice Hall, 1992, pp. 1–2. ISBN: 0-13-473877-2.

[14] S. Ståhl. Clip joint modeling. Diploma work - Department of Applied Mechanics, Chalmers University of Technology, Göteborg, Sweden, no: 2017:27 (2017).

[15] B. Sundström. *Handbok och formelsamling i hållfasthetslära.* Stockholm: Institutionen för hållfasthetslära, Tekniska högsk., 1998, p. 22.

[16] L. Wetterberg. *Personal communication.* Gothenburg, May 21, 2018.

[17] P. Wriggers. *Computational contact mechanics.* Springer, 2006, pp. 17–18. ISBN: 3540326081, 9783540326083.

Appendices

A FE-analysis techniques

In this Appendix the theory behind the two different analysis techniques used during FE-modelling in this project are explained.

A.1 Static analysis with implicit time integration

A static analysis is independent of time and based on the equation of static equilibrium which can be written as discussed in Chapter 3.4 in [11]:

$$\mathbf{0} = \boldsymbol{f}_{ext} - \boldsymbol{f}_{int} \tag{A.1}$$

where $\boldsymbol{f}_{ext}$ is the external force vector and $\boldsymbol{f}_{int}$ is the internal force vector. The meaning of an implicit time integration scheme is that each incremental solution is calculated based on information at the same increment. Since most FE-models generated in Abaqus/Standard are generally non-linear, iteration is needed and by default Abaqus uses Newton's method for this purpose [5]. The aim of the iterations is to find a displacement vector, $\boldsymbol{u}$, at each time increment such that the residual force vector, $\boldsymbol{g}$, is below a certain tolerance:

$$\boldsymbol{g} = |\boldsymbol{f}_{ext} - \boldsymbol{f}_{int}| \ < \ TOL \tag{A.2}$$

Newton's method consists of first making an initial guess of the displacement vector at iteration k, $\boldsymbol{u}^{(k)}$, and then update this solution by adding an incremental displacement vector, $\delta\boldsymbol{u}$, as follows:

$$\boldsymbol{u}^{(k+1)} = \boldsymbol{u}^{(k)} + \delta\boldsymbol{u}^{(k)} \tag{A.3}$$

where $\delta\boldsymbol{u}^{(k)}$ is calculated by inversion of the tangent stiffness matrix, $\boldsymbol{K}_T(\boldsymbol{u}^{(k)})$:

$$\delta\boldsymbol{u}^{(k)} = -\boldsymbol{K}_T^{-1}(\boldsymbol{u}^{(k)})\boldsymbol{g}(\boldsymbol{u}^{(k)}) \tag{A.4}$$

This procedure is repeated until Equation A.2 is fulfilled as discussed in chapter 2.4 in [11].

The advantage of using this analysis type is that it is unconditionally stable which means that the numerical stability is not dependent on the size of the time increment. Furthermore the results accurateness is assured since equilibrium is guaranteed. The disadvantage is that each iteration requires inversion of the tangent stiffness matrix which is a relatively expensive process in terms of computational time [9]. Furthermore numerical problems may arise as the tangent stiffness matrix approaches zero which is common in cases involving a lot of contact and snap-through effects.

A.2 Dynamic analysis with explicit time integration

A dynamic analysis is dependent on time and based on the equation of motion which can be written as

$$\ddot{\boldsymbol{u}} = \boldsymbol{M}^{-1} \cdot (\boldsymbol{f}_{ext} - \boldsymbol{f}_{int}) \tag{A.5}$$

where $\ddot{\boldsymbol{u}}$ is acceleration, $\boldsymbol{M}$ is the lumped mass matrix, $\boldsymbol{f}_{ext}$ is the external force vector and $\boldsymbol{f}_{int}$ is the internal force vector. The acceleration is solved for at the beginning of each increment, then an explicit time integration, the central difference scheme, is used to calculate the velocity at increment $(i + \frac{1}{2})$:

$$\dot{\boldsymbol{u}}^{(i+\frac{1}{2})} = \dot{\boldsymbol{u}}^{(i-\frac{1}{2})} + \frac{\Delta t^{(i+1)} + \Delta t^{(i)}}{2}\ddot{\boldsymbol{u}}^{(i)} \tag{A.6}$$

The displacements for the next increment can then be calculated:

$$\boldsymbol{u}^{(i+1)} = \boldsymbol{u}^{(i)} + \Delta t^{(i+1)}\dot{\boldsymbol{u}}^{(i+\frac{1}{2})} \tag{A.7}$$

This time integration scheme is explicit since only known values from previous increments are used to calculate the displacements at the next increment. This means that no iteration is needed and the increments is relatively inexpensive in terms of computational time, as discussed in chapter 2.4.5 in [6].

One disadvantage with the explicit time integration scheme is that it is not unconditionally stable. The stable time increment is determined by the time it takes for a dilatational wave to travel through the smallest element, thus the maximum stable time increment is determined by the smallest element, as described in chapter 2.4.5 in [6]. The required amount of increments is thus often larger than for an implicit analysis.

This type of analysis technique is effective for analyses involving a lot of contact and sliding between parts where an implicit analysis would experience convergence issues.

B Boundary conditions used for evaluation of torsional stiffness

During numerical evaluation of torsional stiffness different boundary conditions for the part of front sill moulding where used for each rotation. The boundary conditions for rotation around X,Y and Z are presented in Figures B.1, B.2 and B.3 respectively. The resulting applied torque presented in Chapters 3.6.1 and 3.7.1 was calculated by use of the average torque arm length. The torque arm length for each rotation at start and end of rotation as well as the average can be seen in Table B.1.

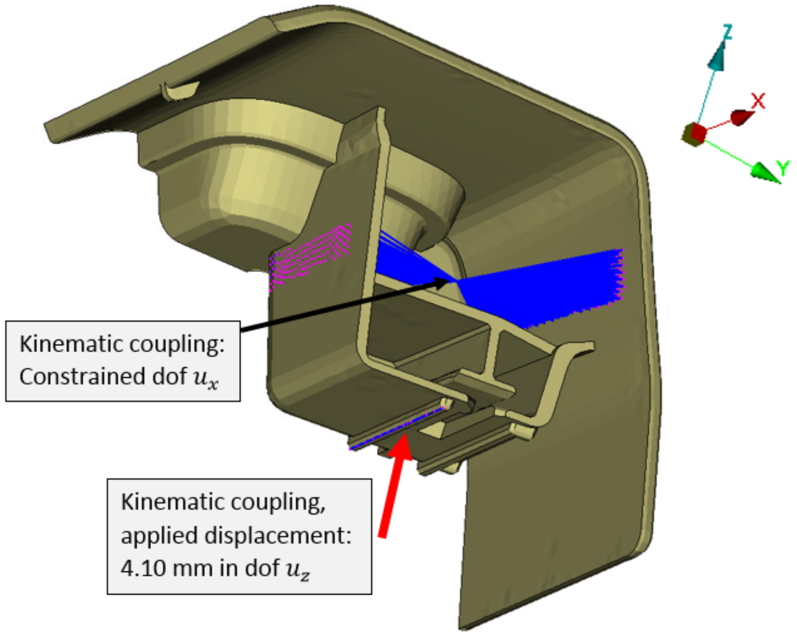

Figure B.1: *Boundary conditions and applied displacement for the panel, rotation around X.*

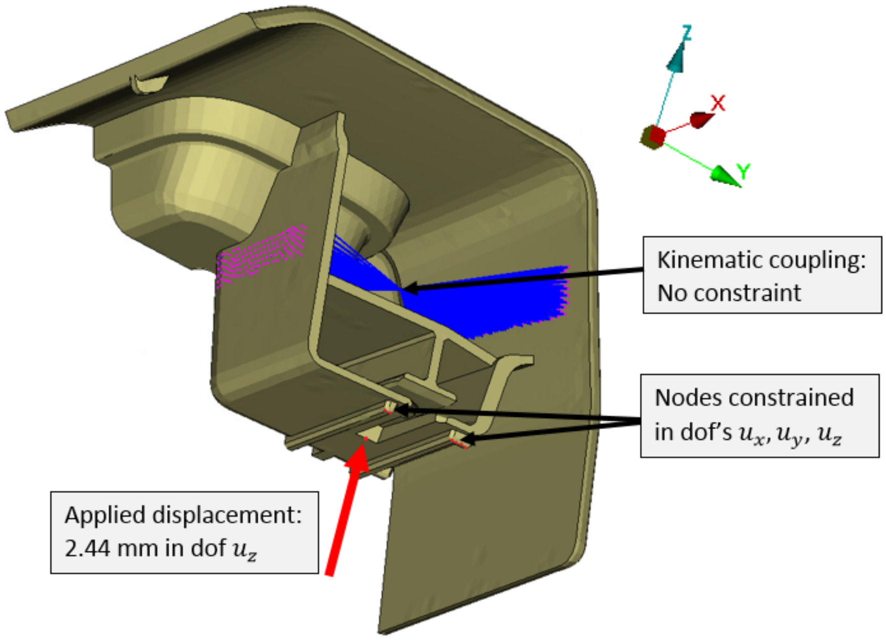

Figure B.2: *Boundary conditions and applied displacement for the panel, rotation around Y.*

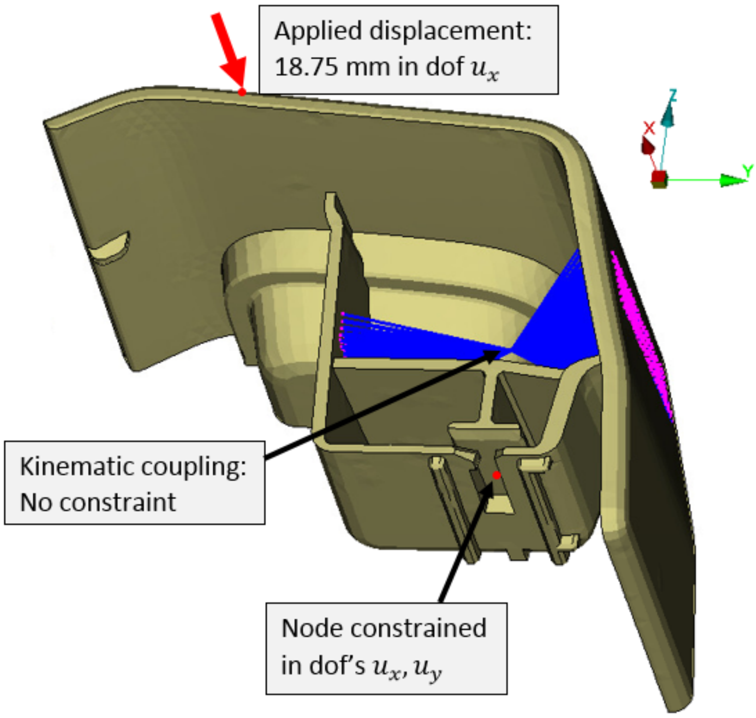

Figure B.3: *Boundary conditions and applied displacement for the panel, rotation around Z.*

Table B.1: Torque arm length at start and end of rotation as well as average torque arm length.

Load case:	L_1 $[mm]$:	L_2 $[mm]$:	L_{avg} $[mm]$:
X-rotation	6.00	5.70	5.85
Y-rotation	5.88	5.45	5.67
Z-rotation	42.20	30.40	36.30

C Numerical validation of assembly process FE-model

Since equilibrium is not guaranteed when adopting an explicit time integration scheme the validity of the assembly simulation was checked by an investigation of the energies and reaction forces during the analysis.

C.1 Energy analysis

In order to assure that the behaviour during analysis of the assembly process is physically realistic the energies during the simulation was checked. The energies during the assembly process can be seen in Figure C.1. Energy from external work is directly related to the external forces acting on the parts included in the simulation. The internal energy is defined as energy from strains that are present in the parts. Frictional dissipation is the energy that is generated from parts sliding relative to each other. The kinetic energy is based on the velocity of the parts and the magnitude of artificial strain energy is related to hourglass effects, e.g. unphysical strain behaviour.

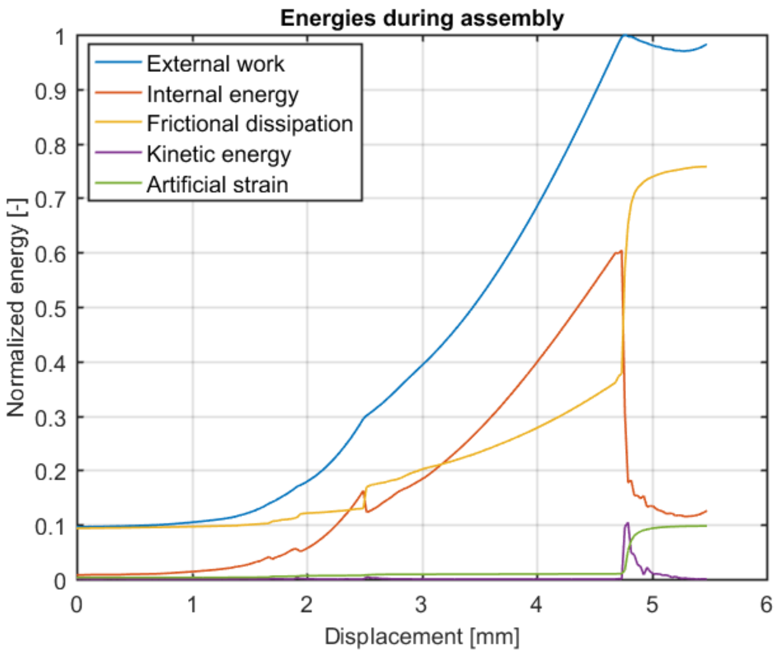

Figure C.1: *Energies during assembly.*

As can be seen in Figure C.1 the Internal energy increases until approximately 2.5 mm displacement where it suddenly drops. The reason for this behaviour is that strain is built up as sticking friction between the clip and plate is present. When the maximum allowed shear stress for sticking friction is reached the strain is suddenly released and consequently the clip accelerates which give rise to a sudden increase in frictional dissipation energy.

The internal energy then increases again as strain builds up when the clip is laterally compressed. Since this strain give rise to increased normal forces between the clip and the plate frictional dissipation also increases. This increase is seen until the clip waist have passed the hole and then the internal energy drops as the clip experience snap through effect.

The artificial strain energy is low until the clip waist passes the plate and accelerates due to a snap-through effect. The main part of interest is the force until the clip reaches the second peak and a good rule of thumb is that the artificial strain energy should not exceed 5% in order for an acceptable amount of hourglass effects which is satisfied in this region.

C.2 Plate constraint reaction force analysis

In order to further increase the confidence in the accurateness of the assembly-simulation the reaction forces where the plate is constrained from movement was investigated. Since equilibrium is not a criteria when performing an analysis with explicit time integration this is one way of checking this. The reaction force in Z-direction for the plate compared to the assembly force can be seen in Figure C.2. The behaviour of the plate reaction force is very similar to the assembly force thus providing an indication that equilibrium is approximately satisfied in the direction of assembly.

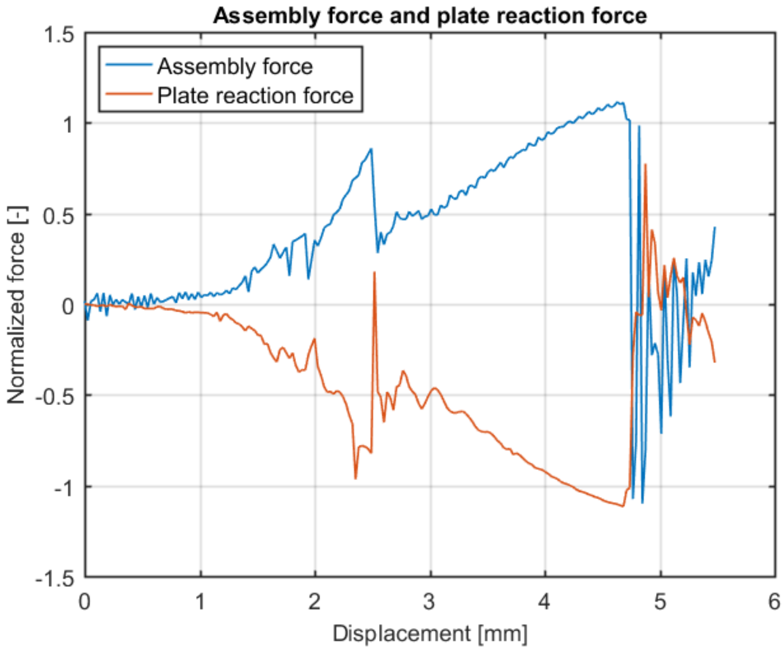

Figure C.2: *Assembly force compared to the reaction force in Z-direction of the nodes where the plate is constrained from movement.*